# The contribution of the Indo-Pacific sea surface height variability to the Indonesian Throughflow under changing climate.

Ph.D. Thesis Submitted by

**Shilimkar Vivek Kishor**

Ph.D. Supervisor

**Prof. Youichi Tanimoto**

Division of Earth System Science

Graduate School of Environmental Science

Hokkaido University, Sapporo, Japan

**9 November 2022**

# Contents

# Abstract

The Indonesian throughflow (ITF) transports a significant amount of warm freshwater from the Pacific to the Indian Ocean, making it critical to the global climate system. This study examines decadal ITF variations using ocean reanalysis data as well as climate model simulations from the Coupled Model Inter-comparison Project Phase 5 (CMIP5). While the observed annual cycle of ITF transport is known to be correlated with the annual cycle of sea surface height (SSH) difference between the Pacific and Indian Oceans, ocean reanalysis data (1959–2015) show that the Pacific Ocean SSH variability controls more than 85% of ITF variation on decadal timescales. In contrast, the Indian Ocean SSH variability contributes less than 15%. While those observed contributions are mostly reproduced in the CMIP5 historical simulations, an analysis of future climate projections shows a 25%–30% increase in the Indian Ocean SSH variability to decadal ITF variations and a corresponding decrease in the Pacific contribution. These projected changes in the Indian Ocean SSH variability are associated with a 23% increase in the amplitudes of negative zonal wind stress anomalies over the equatorial Indian Ocean, along with a 12$^{o}$ eastward shift in the center of action in these anomalies. This combined effect of the increased amplitude and eastward shift in the zonal wind stress increases the SSHA variance over the Indian Ocean, increasing its contribution to the ITF variation. The decadal ITF changes discussed in this study will be crucial in understanding the future global climate variability, strongly coupled to Indo-Pacific interactions.

**Keywords**: Indonesian throughflow, sea surface height, wind stress, wind stress curl, Indian ocean, Pacific ocean, future climate, air-sea interaction, decadal variability, climate change.

# Acknowledgments

I used to think the acknowledgment part was just for the formality of the thesis. However, these few years of my Ph.D. changed my thinking completely. The journey of pursuing a doctorate has been through many ups and down, academically, socially, and personally. My Ph.D. work could not have been possible without people's support, not only in hard times in my life but also in day-to-day life.

First and foremost, I would like to express my sincere gratitude to my advisor Prof. Youichi Tanimoto, for supporting my research. Words cannot express my feelings toward my professor for his invaluable patience and feedback. His office has always been open for discussion despite his busy schedule, unlike many Ph.D. advisors. Additionally, this part of my life would not have been possible without the generous support from the Ministry of Education Culture, Sports, Science, and Technology - the Japanese Government.

Besides my advisor, I would like to thank Dr. Hiroto Abe for sharing his reduced gravity model for my research. Research carried out with his model is an integral part of my research and thesis; without this model, my research would be incomplete. In addition, his insightful comments and discussion of my research have been essential building blocks for my thesis.

During the Ph.D., maintaining the work-life balance is very important. That was only possible with the support of my parents remotely and with the presence of my wife (Anita), daughter (Anvi), and friends - Jagjit, Rahul, Chetna, and Dr. Ram.

Lastly, I am grateful to the Minato family in Sapporo, who accepted me as one of the family members with whom I spent 6 months living in their house. A house that became

home in a very short time, and eventually, I became a part of the family. Their unconditional love and kindness made my life very cheerful during my stay with them. I don't think I would have completed the Ph.D. without their support. I will definitely pay the love and kindness forward.

# List of Figures

**Figure 2.1**: Typical Indonesian Throughflow transport geography

**Figure 2.2** Time series of the ITF volume transport in Makassar Strait (black curve) and near IX01 line (red curve) (1 Sv=10 $m^6$ $s^{-1}$) based on the ORAS4. The transport is calculated by vertically integrating the monthly mean velocity from the surface to 1000-meter depth in Makassar Strait and the surface to the depth above the bottom from Australia to Indonesia between 9°S and 20°S along 115°E (near IX01). A 13-month (85-month) running mean was applied on the thin curve (thick curve).

**Figure 2.3** (a) A map of correlation coefficients (contoured for every 0.2) in the decadal SSHA onto the decadal volume transport variation near IX01 line as in Fig. 2.1. The coloring convention is shown on the right of the panel. Regions in the inset black rectangles are the NWP (6–16°N, 125–155°E), EEIO (5°S–5°N, 65–95°E), and SEI (6–16°S, 85–115°E) regions selected for the calculation of the SSHA difference. (b) as in (a) but for regression coefficient (contoured for every 10 cm/Sv).

**Figure 2.4**(a) Time series of the decadal SSHA (cm) over the NWP region based on the ORAS4 (thick black curve) and AVISO (blue curve). (b) As in (a), but for the SEI region (solid curves) and the EEIO region (dashed curves).

**Figure 2.5** Time series of the decadal ITF transport anomalies (Sv, black line) and the SSHA difference (cm) across the NWP–SEI regions (blue solid curve), and across the NWP–EEIO regions (blue dashed curve) based on the ORAS4 reanalysis. The estimated SSHA difference across the NWP–SEI regions are also superimposed (light blue solid curve). The axis for the ITF

transport is on the panel's left side, and the SSHA difference's axis is on the right.

**Figure 2.6** (a) Time series of the decadal SSHA (cm) in the NWP region based on the ORAS4 ("direct" SSHA by black curve), reduced gravity model forced by the ORA-S3 wind stress curl ("estimated" SSHA by blue curve), and AVISO (red dashed curve). (b) as in (a), but for the wind-forced component (blue thick curve) and the boundary condition component (blue dashed curve) in the estimated SSHA.

**Figure 2.7** As in Fig. 2.6, but for the SEI region.

**Figure 2.8** A map of correlation coefficients on a decadal timescale (contoured for every 0.2) in zonal wind stress anomalies in ORA-S3 onto the effect of boundary condition SSHAs averaged over the SEI region based on the ORAS4. The coloring convention is shown on the right of the panel.

**Figure 2.9** Time series of the boundary condition component (blue dashed curve) in the estimated SSHA by the reduced gravity model (same as in Fig. 2.7b) and the calculated boundary condition contribution to the SSHA in the SEI region using a regression analysis with the equatorial (5$^{o}$N–10$^{o}$S, 65–105$^{o}$E) zonal wind stress of the ORA-S3 (solid black curve).

**Figure 3.1:** Time series of the decadal SSHA difference (cm) across the NWP–SEI regions, based on the simulated direct SSHA in the selected CMIP5 models (black curve) and the estimated SSHA (red curve) by using the simulated wind stress of those models. Simultaneous correlation

coefficients between those direct and estimated SSHAs are indicated on each panel's upper right corner.

**Figure 3.2:** Same as Fig. 3.1 (a) but for not-selected CMIP5 models.

**Fig. 4.1** (a) Composite maps of the difference between positive and negative phases of the decadal SSHA (contoured for every 1.0 cm) based on the ORAS4 dataset. (b) As in (a), but for the multi-model ensemble, decadal SSHA in the historical simulations of the selected CMIP5 models. (c) As in (a), but for the decadal SSHA in the RCP8.5 simulations of those models. The coloring convention is shown on the right of the panels, respectively.

**Fig. 4.2** (a) Difference composite maps of the decadal wind stress curl anomalies (contoured for every 0.2 N $m^{-3}$) based on the multi-model ensemble mean of selected CMIP5 historical simulations. The overlayed box 125°E-165°W, 6-16°N indicates the atmospheric region that affects the SSHA variability in the NWP region. The coloring convention is shown on the right of the panels. (b) As in (a), but for the simulations under the RCP8.5 scenario. (c) is the difference between (b) and (a).

**Fig. 4.3** As in Fig. 4.2, but for zonal wind stress anomalies (contoured for every 0.5 N $m^{-2}$) and the overlayed box 65-105°E, 5°N-10°S indicates the atmospheric region that affects the SSHA variability in the SEI region.

# List of Tables

**Table 4.2** Difference composite values of the direct and estimated SSHAs in the NWP and SEI regions based on the ORAS4 and the multi-model ensemble mean of the selected CMIP5 models with their standard deviation. The bottom row indicates the future changes of the composite values from the historical simulation to the future simulations under the RCP8.5 scenario.

# Chapter 1: General Introduction

## 1.1 Indonesian throughflow

The Indonesian Throughflow (ITF) transports a considerable volume of seawater from the warmer and less saline western tropical Pacific to the colder and more saline southern tropical Indian Ocean via the straits of the Indonesian Archipelago. Wyrtki (1987) put forward a theory that the sea surface height (SSH) difference between the North-Western Pacific Ocean (NWP) and South-East Indian Ocean (SEI) drives the ITF. Although this method cannot give a numerical value for the ITF, it can track the ITF variability. This method could track the seasonal variation of ITF to a reasonable extent; however, it could not explain ITF transport's inter-annual variation and did not correlate with the El Niño Southern Oscillation (ENSO). Later, the ITF volume transport was measured within the Indonesian Seas. Observations show that a significant part of ITF is derived from the North Pacific Ocean through the Makassar Strait. Another passage for transporting the South Pacific Ocean's deep water to the Indian Ocean is the Lifamatola passage, east of Sulawesi Island. Before entering the Indian Ocean, the Indonesian throughflow's salinity and the temperature changes in the Banda Sea; it is then funneled into the Indian Ocean through the three major outflow passages, namely, Lombok, Ombai, and Timor passages.

Observational estimates during 1996-1997 and 2004 to 2006 show that the net ITF volume transport from the Pacific to the Indian Ocean through the major straits of the Indonesian Archipelago is about 15 Sverdrup (Sv, 1 Sv = $10^6 m^3 s^{-1}$), with seasonal variations ranging between 0.5 to 2.5 Sv (Gordon et al. 2008; Sprintall et al. 2009). Observational estimates in different ITF inflow and outflow straits are listed in Table 1.1. These observations show that about 80% of ITF's inflow passes through the Makassar Strait (Gordon et al. 2008;

Lee et al. 2015). Sizeable interannual variability in the total ITF with a typical amplitude of 3.0 to 3.7 Sv is also reported based on hydrographic observations and numerical modeling studies (Susanto et al. 2012; Gordon et al. 2008, 2010; Meyers 1996; Sprintall and Revelard 2014, Potemra et al. 2007). These ITF fluctuations lead to the basin-scale temperature variations in the ocean surface and subsurface layers in the Indian Ocean, which in turn modulates the climate variability over the many countries along the Indian Ocean coast via the ocean-atmosphere interaction (Lee and McPhaden 2008; Murtugudde et al. 1998; Potemra and Schneider 2007; Schneider 1998; Song et al. 2007; Tokinaga et al. 2012).

**Table 1.1**: Observational estimates of the ITF in different inflow and outflow passages/straits within the Pacific and Indian Oceans (Gordon et al. 2008)

| Year | Inflow passages in Pacific Ocean | | Outflow passages in Indian Ocean | | |
|---|---|---|---|---|---|
| | Makassar Strait | Lifamatola Strait | Lombok Strait | Ombai Strait | Timor Passage |
| 1997 | 9.2 Sv | 1.5 Sv | 1.7 Sv | 4.5 Sv | 4.3 Sv |
| 2004-2006 | 11.2 Sv | 1.1 Sv | 2.5 Sv | 4.9 Sv | 7.5 Sv |

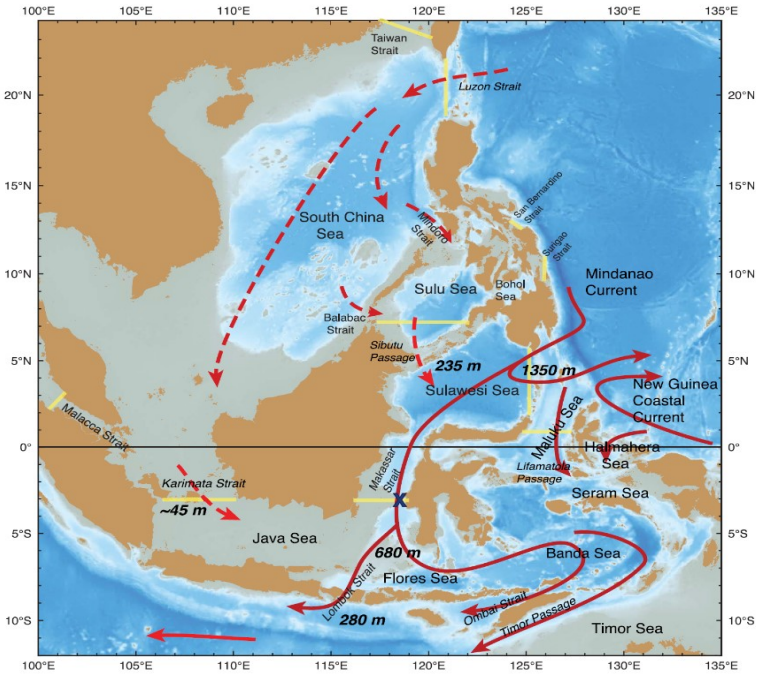


**Figure 1.1**: Schematic of the Indonesian throughflow (solid red arrows) and the South China sea throughflow circulations. Topographic sill depths are given in black italics. The X indicates the Makassar Strait mooring site.

## 1.2 Inter-annual variation of the Indonesian throughflow

The pressure gradient in the ocean surface layers across the straits drives the ITF. Hence, the sea surface height (SSH) difference between the NWP and the SEI is an excellent measure to represent ITF transport (Wyrtki 1987). The large-scale surface winds maintain this SSH difference between the tropical Pacific and the Indian Ocean. Climatological surface easterlies over the tropical Pacific associated with the Hadley and Walker circulations pile up the surface waters and form the higher SSH in the NWP region than the relatively lower SSH in the SEI region. Since the SSH in the SEI region is controlled by the climatological Indian Monsoon (Han et al., 2014), the surface winds' seasonal reversal can contribute to the seasonal ITF variations. Besides this climatological view, the modulation of these surface winds on the interannual and decadal timescales can induce ITF fluctuations by changing the SSH difference between the NWP and SEI regions.

After Wyrtki (1987) put forward his theory of ITF transport, many studies tried to identify the crucial processes that control the ITF transport variation. Potemra et al. (1997) used a model and observed data inter-comparison to derive and determine the feasibility of deriving an index to estimate variation in ITF transport from the Pacific to the Indian Ocean. Authors used a sea level in four Pacific and Indian Oceans regions, two more than Wyrtki (1987) suggested. Sea level at Davao and warm pool in the Pacific Ocean, Darwin, and the south coast of Java in the Indian Ocean were used to develop the ITF variability index. Sea level anomalies from these four locations fit the model ITF transport anomalies using multiple regression techniques explained in Chelton (1983). The authors found that the Pacific Ocean controls the large-scale pressure gradient forcing of the throughflow on an interannual timescale.

In contrast, the Indian Ocean has a small contribution. Potemra (2007) revisited the

same question with the new approach. Sea-level changes were allowed to lead or lag the ITF signal to account for the time needed for the signal to pass through the ocean basins. The resultant ITF variability does not correlate with the ENSO.

Few studies show some correlation between ENSO and ITF transport. Meyers (1996) used a twelve-year expendable bathythermograph (XBT) hydrological data (1983-1994) near the ITF outflow region in the Indian Ocean to construct an ITF variability record. ITF showed significantly higher transport during one of the La-Niña events. However, no significant change in variation is observed during the El Niño events. England and Huang (2005) explored ITF variation and ENSO index relationship using a model dataset. ENSO index can be calculated in different regions; they used a Niño-3 index for their analysis. ITF transport calculation was carried out at two locations, along the 4$^{o}$S and another along the 115$^{o}$E from south Java coast to Australia's east coast. The mean and interannual variation of ITF is the same in both locations. Analysing the ITF transport and Niño-3 index, the authors show that ITF transport and Niño-3 index have a negative correlation coefficient of -0.19 at zero lag. The maximum correlation reaches -0.32 while ITF lags the Niño-3 index by nine months. Similarly, several studies (Potemra 2005, Meyers 1996, England and Huang 2005) also indicated that the ITF transport negatively correlates with the ENSO on the interannual timescale. These studies also tried to explain the negative correlation between ITF variation and ENSO by inter-annual wind variation. The increased ITF transport during the La-Niña event was explained by the stronger easterly winds and elevated sea surface height in the western Pacific Ocean, which increased the pressure gradient between the Pacific and Indian Oceans, funnelling more water from the Pacific Ocean. The opposite mechanism is expected to decrease the ITF during El Niño events. However, the results were not consistent among the studies. In addition, the ITF variation study based on six years period (July 1992 – June 1997) shows a high correlation of interannual

ITF variation with the equatorial Indian Ocean winds (Masumoto 2002). However, the ITF variation is not correlated well with the ENSO index on the interannual timescale in comparison to other studies. The reason for not getting consistent results for the correlation between ITF and ENSO index could be due to the fact the correlation analysis was done for different periods.

The Indian Ocean also influences the ITF transport via remotely forced Kelvin Waves triggered by the equatorial Indian Ocean winds (Masumoto 2002; Sprintall et al. 2009; Drushka et al. 2010). Potemra and Schneider (2007), using the model dataset, showed that the inter-annual variation of the ITF is caused not only by the ENSO but also by the equatorial Indian Ocean wind variation associated with the Indian Ocean Dipole (IOD) events. In terms of ITF variability, the ENSO and IOD events acts contrary to each other. These events act to increase (La Niña and Negative IOD) or decrease (El Niño and Positive IOD) SSH in the NWP and SEI regions simultaneously, resulting in no significant change in ITF variation, depending upon the type and strength of wind anomalies of an event. A similar conclusion was obtained by Sprintall and Revelard (2014). The authors used daily observed velocity data in three major outflow passages of ITF and the daily satellite observed SSH (AVISO). Daily SSH was then regressed over the daily observed volume transport in the upper and lower layer of three different passages to create a longer proxy ITF record. Newly developed proxy ITF transport in the upper and lower layer of three major outflow passages of ITF in the Indian Ocean was then analysed for its dependence on ENSO and IOD variation on the interannual timescale.

The zonal wind stress in the tropical Pacific and the Indian Ocean negatively correlates with the inter-annual timescale. During the ENSO events, the wind anomalies over the Indian Ocean can alter the SSH in the south-eastern Indian Ocean, off the Java and Sumatra islands. The variation in the south-eastern Indian Ocean is in phase with the western north Pacific on

the interannual timescale, which contributes to the weakening of the pressure gradient generated by the SSH variation in the western north Pacific, resulting in minor ITF anomalies (Masumoto 2002; Murtugudde, Busalacchi, and Beauchamp 1998; Potemra and Schneider 2007; Sprintall et al. 2014). Hence, it is still an open question to understand the relative contribution of the Pacific Ocean and the Indian Ocean to the ITF transport on the interannual and longer timescale (Sprintall et al. 2014).

Figure 1.2 show the anomalous SST and wind conditions during the La Niña and El Niño conditions over the tropical region, which helps understand the dynamics behind the above explanation. While green and orange colour in the plot indicates the global SST anomalies during the La Niña and El Niño conditions, the overlying navy-blue colour indicates the associated anomalous Hadley cycle. Large scale convergence (divergence) during the La Niña (El Niño) condition results in increased (decreased) SSH anomalies in the south-eastern Indian Ocean and western-north Pacific Ocean simultaneously. These covarying SSH anomalies over these regions does not affect the SSH difference between NWP and SEI regions, hence the resultant ITF variability remains unaffected.

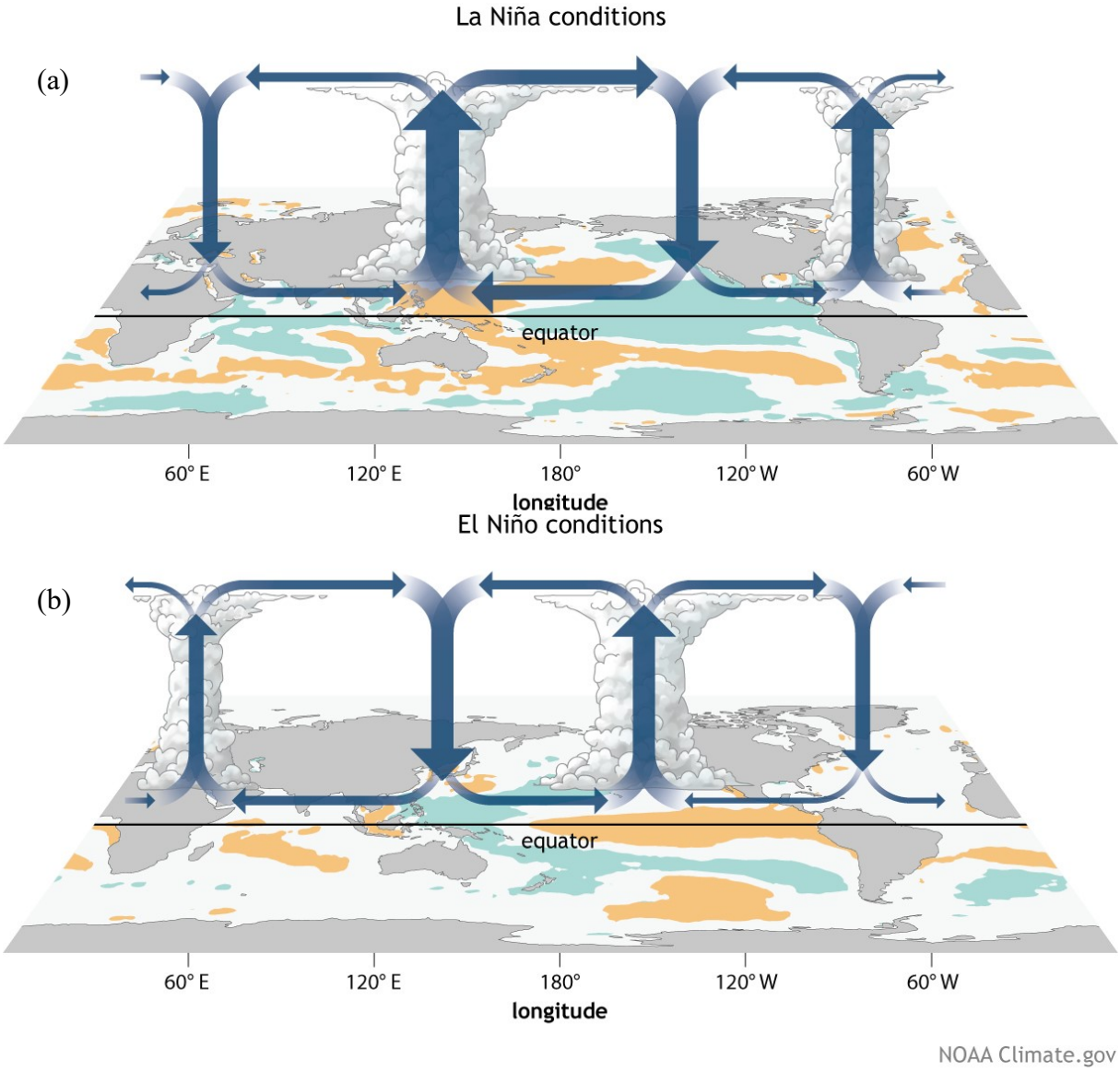


**Figure 1.2**: Generalized Walker Circulation (December-February) anomaly during La Niña (El-Niño) events in Fig.1.2b (Fig.1.2a), overlaid on a map of average sea surface temperature anomalies. Anomalous ocean cooling (blue-green) (warming (orange)) in the central and eastern Pacific Ocean and warming (cooling) over the western Pacific Ocean enhance the rising branch of the Walker circulation over the Maritime Continent and the sinking branch over the eastern Pacific Ocean. Enhanced rising (sinking) motion is also observed over northern South America, while anomalous sinking (rising) motion is found over eastern Africa.

**Source: NOAA Climate.gov drawing by Fiona Martin**.

## 1.3 Decadal variation of the ITF and objectives of the thesis

Lee and McPhaden (2008) mentioned that the negative correlation of the surface winds over the two basins is also found in the recent inter-decadal change between 1993-2000 and 2000-2006, indicating a little effect on the SSH difference across the Indonesian Archipelago straits during that time. Contrary to the similarity of inter-annual and decadal timescales, Nidheesh et al. (2013) show that the variation of winds over the Pacific and the Indian Ocean on the decadal timescale is relatively independent for longer timescale (1959-2009). The inconsistency in results among the previous studies may arise from the following reasons such as the varying relationship between the Pacific and Indian Oceans in different decades (Han et al., 2014), limited duration of the available satellite observations (Han et al., 2014) and/or different representations of the long-term variability in the Indian Ocean atmospheric reanalysis data sets (Nidheesh et al. 2013).

Nidheesh et al. (2013) also show that the simulated SSH anomalies in the ocean general circulation model's dominant spatial patterns are different between interannual and decadal time scales (Fig. 1.3, imported Fig.6 from Nidheesh et al., 2013). While the leading mode of the SSH anomalies on the interannual time scale displays comparable loadings across the straits of the Indonesian Archipelago and, therefore, the unchanged SSH gradient between the NWP and SEI regions, the one on the decadal time scale depicts significant loadings in the NWP region with subtle loadings in the SEI region. Hence, the SSH difference across the Indonesian Archipelago straits associated with this decadal leading mode can significantly contribute to the decadal ITF variations. These significantly different loadings between the NWP and SEI regions on the decadal timescale suggest different contributions from the decadal SSH variations in the NWP and SEI regions, respectively, to the decadal ITF variation. A recent study by Li et al. (2018) constructed the multidecadal ITF time-series based on the

observed and reanalysis of surface wind only over the North Pacific Ocean, showing the significant contribution of the surface winds over the tropical Pacific to the ITF variation.

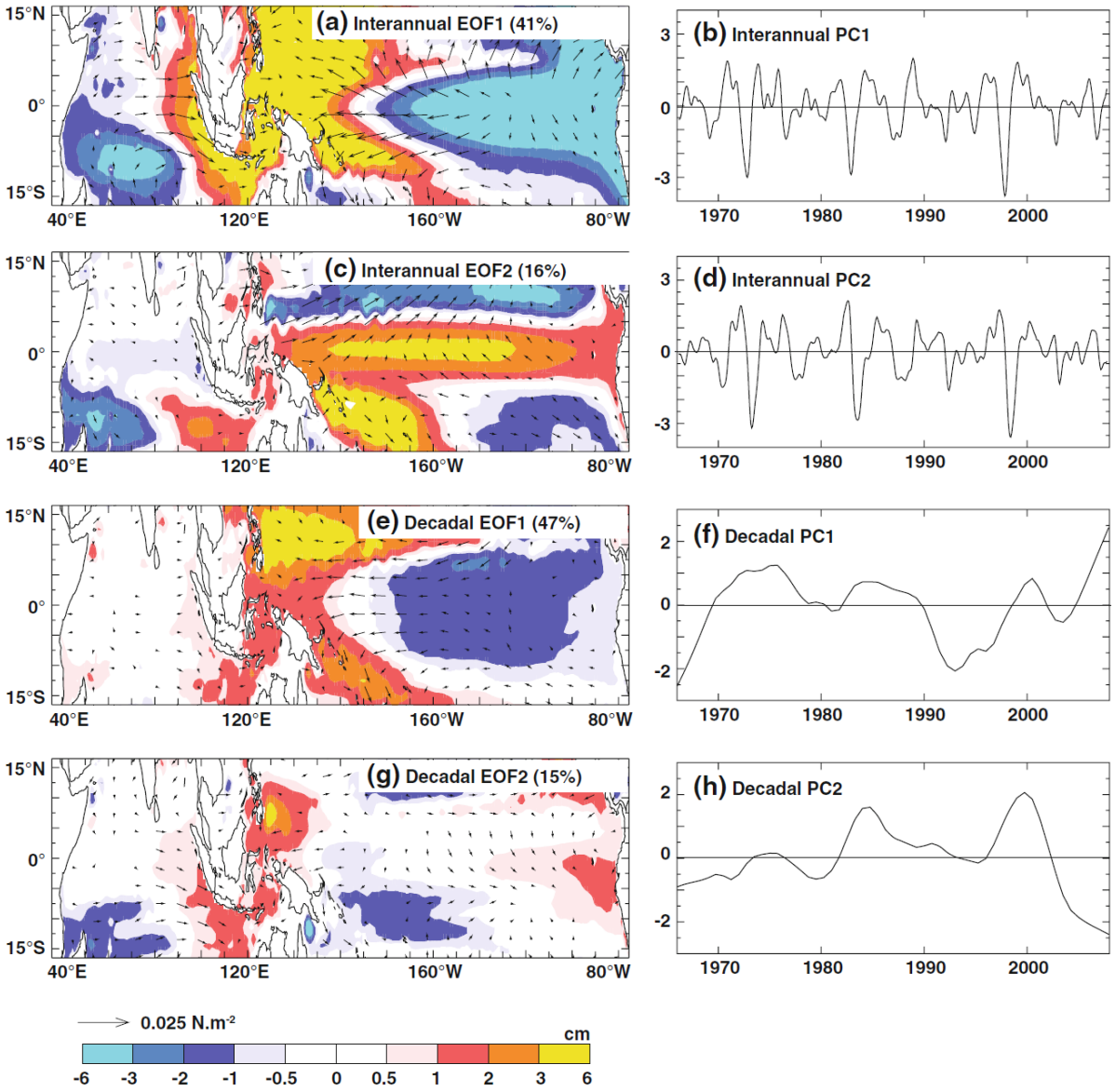


**Figure. 1.3**: First two EOF patterns of the model steric sea level anomalies over the Indo-Pacific sector (left column) and their corresponding normalized principal components (right column) at interannual (a–d) and decadal timescales (e–h). The arrows display the wind stress components regressed onto each normalized PCs. The percentage variance explained by each EOF is shown in brackets. Units are in cm for EOF patterns.

## 1.4 Purpose and outline of the thesis

Due to global warming, the fundamental basement changes in the climate system can affect the behaviors of perturbations around the mean state. These changes will alter the decadal ITF variation and the relative contributions of the decadal SSH variations over the NWP and SEI regions to the ITF. Analysis of the future climate projections by CMIP5 models consistently shows increased SST variances of the SEI region due to the shallowing of the thermocline in the eastern equatorial Indian Ocean (Cai et al., 2013). These changes in the SST may lead to changes in the winds over the Indian Ocean region, which affects the SSH variation of the underlying region. Hence, this study aims to understand the relative contribution of decadal SSH variability over the Pacific and Indian Oceans to a decadal ITF variation and assess the dynamics behind the contribution changes in a future climate. CMIP5 models cannot resolve the Indonesian Archipelago that limits the direct calculation of the ITF transport based on the simulated velocity in the ocean. To overcome this inability of CMIP5 models, we provide a new method of estimating the SSH difference using only observed and reanalysis of atmospheric wind forcing of the Pacific and Indian Oceans to obtain the proxy ITF and the estimation based on inter-ocean SSH difference.

The objectives described above are achieved after creating a climatological base for CMIP5 data using Ocean Reanalysis System-4 (ORAS4) and Ocean Reanalysis System-3 (ORA-S3) ocean reanalysis datasets (Balmased et al 2008, Balmaseda et al 2013). Figure 1.4 explains the flow of the research. The observed in-situ ITF volume transport data is available for short time. Hence the reproducibility of ITF in the long-term ORAS4 reanalysis dataset was compared with in-situ observed data in chapter 2. In section 2.2 the inter-comparison of the in-situ observed data and ORAS4 reanalysis data confirms that ORAS4 reanalysis has a good skill in capturing the ITF variability. Further in section 2.3.1 with the correlation and regression

analysis between ITF volume transport and direct SSHA in ORAS4 reanalysis data is used to calculate the ITF volume transport with SSHA difference between NWP and SEI regions. A new method of estimating the SSHA only with the wind stress from ORA-S3 dataset was discussed in section 2.3.3. The ITF volume transport calculation from estimated SSHA and capability of this method was also discussed in this section.

Using the understanding developed in the above sections, the CMIP5 models were selected based on the climatology of SSH difference between NWP and SEI regions for further analysis in chapter 3. Selected models were later analysed to understand the contribution from NWP and SEI regions' direct and indirect SSHA to the ITF volume transport variation on decadal timescale in historical simulations and future RCP8.5 scenario in section 4.2.1. Finally, the dynamics behind the changes in the future contribution from the NWP and SEI regions are discussed in section 4.2.2. The flow-chart gives the idea as to how the thesis is organised.

The observed data for the ITF volume transport is not available for more than a decade, hence getting the data for analysis of decadal timescale is tricky. Chapter 2 discusses the decadal ITF volume transport based on reanalysis dataset and ITF volume transport calculations based on different methods. Further the chapter 3 discusses the challenges in using the CMIP5 data and the diagnosis we performed for selecting the CMIP5 models for analysis. Chapter 4 discusses the contribution of the Indo-Pacific Sea surface height to the ITF on decadal timescale in the historical simulation and RCP8.5 future scenario. This chapter also discussed the large-scale wind dynamics behind the changes in the contribution from respective ocean regions. Final chapter, chapter 5, concludes the thesis.

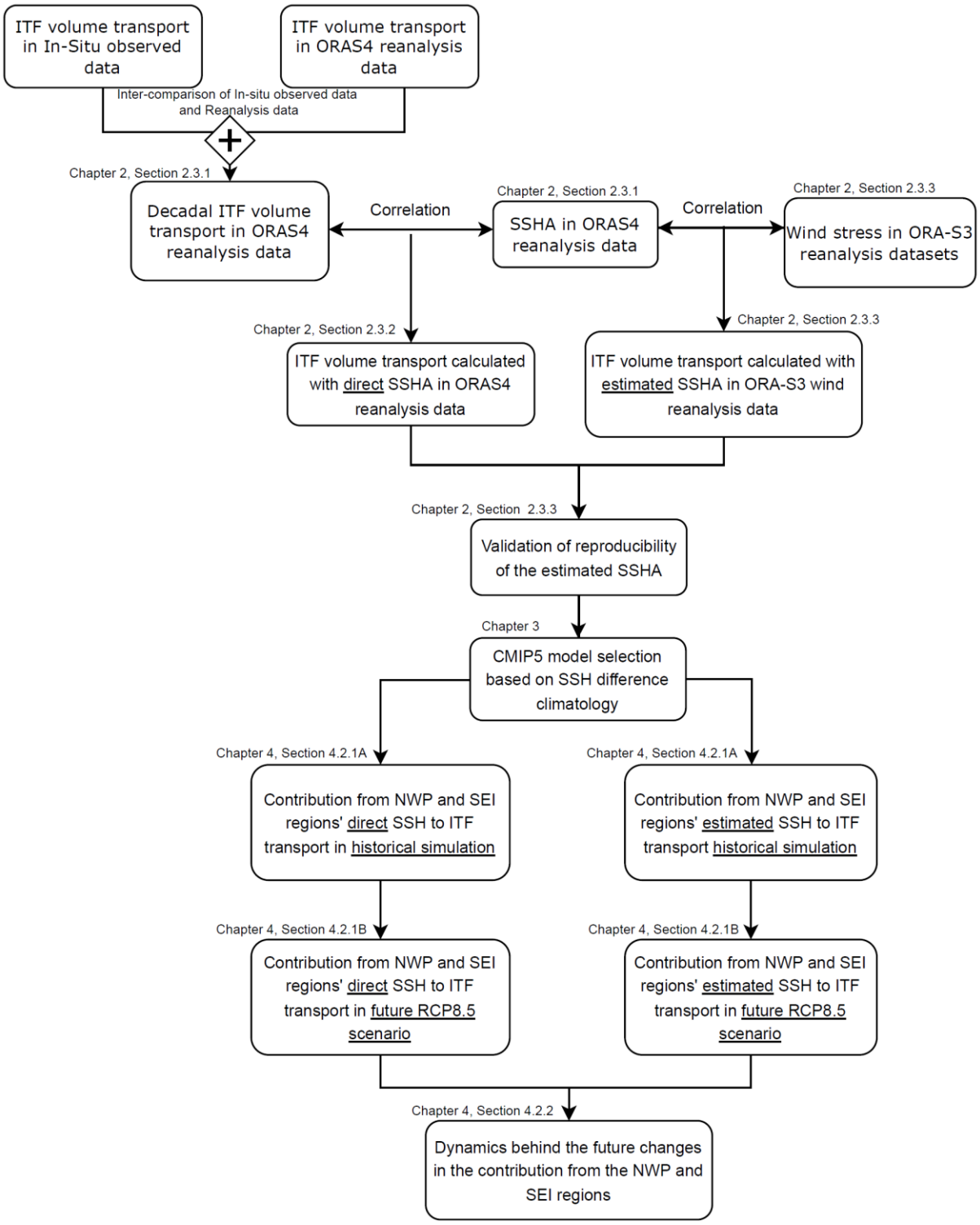


**Figure 1.4**: Flow of the thesis to understand the direction of the thesis clearly.

# Chapter 2: Decadal Indonesian Throughflow (ITF) transport based on simulated velocity in the ORAS4, direct SSH difference and estimated SSH difference.

## 2.1 Introduction

Many studies have attempted to estimate the ITF transport based on inter-ocean pressure or SSH difference from direct observations of volume transport in ITF inflow and outflow passages. Wyrtki (1987) suggested that the SSH difference between Davao (Pacific) and Darwin (Australia) could explain the ITF variation. Later satellite observed SSH data, sophistication, and refinement of numerical models motivated the further exploration of the correlation between SSH and ITF variability using numerical model output (Metzger et al. 2010; Potemra 2005; Potemra and Schneider 2007; Tozuka et al. 2009), ITF transport based on expendable bathythermograph (XBT) (Wijffels et al. 2008; Wijffels and Meyers 2004) and direct observations (Li et al. 2018; Sprintall and Revelard 2014; Tillinger and Gordon 2009).

Longest volume transport observations in one of the major inflow passages, Makassar Strait, of the ITF was conducted only from 2004 to 2011. This data is not long enough for studying the decadal variation of the ITF. Hence, this chapter serves the purpose to select an appropriate region to calculate the ITF volume transport in Ocean ReAnalysis System - 4 (ORAS4) reanalysis dataset (Balmaseda et al 2013). For this purpose, we compared the observed data with the reanalysis data and made sure the reanalysis data has a good skill in Areproducing the ITF volume transport. Further, an attempt will be made to estimate the ITF volume transport with the reanalysis SSH and wind dataset. Although those assimilated and simulated data sets contain the velocity profiles in the ocean surface layers as the output variables, the procedures in the present study only need the large-scale SSH distribution

rather than velocity profiles in the individual Indonesian straits.

Following the previous studies, the same technique of estimating the ITF variation was employed using an SSH difference between the Pacific and Indian Oceans on a decadal timescale. The two sorts of SSH fields, such as "the direct SSHA" and "the estimated SSHA," can be obtained based on the assimilated and simulated data set in the following ways. As the direct SSH field, the SSH field provided as the output variable in the ORAS4 data set is utilized. These SSH fields are utilized to estimate the ITF volume transport as the SSH difference between the NWP and SEI regions since the SSH difference between these two regions has the highest correlation with ITF variation as discussed in the following section. The estimated SSHA is the simulated result of the reduced gravity model forced by only atmospheric wind stress force. The wind stress field from ORA-S3 was utilized to force the reduced gravity model. Two methods of calculating ITF volume transport from the direct and estimated SSH are again explained in Sections 2.3.2 and 2.3.3.

## 2.2 Data and Analysis method

Direct measurements of volume transport of Indonesian throughflow within the Indonesian Islands are available for a limited period. At first the volume transport was calculated under the (ARLINDO) program from November 1996 to July 1998 in major inflow and outflow passages of Indonesian Throughflow (Gordon and Ffield 1999). Figure 1.1 (imported Fig.1 from Gordon et al., 2010, with slight modification in caption) shows the geography of the Indonesian Islands and the locations of the moorings. Continuous observations in the same passages were carried out from January 2004 to December 2006 under the INSTANT program (Gordon et al. 2010; Sprintall et al. 2004). Later, the observations in the primary inflow passage Makassar Strait were continued with the Monitoring Indonesian Throughflow Program (MITF) (Gordon et al. 2012) from 2006 to 2011 and 2014 to 2015.

However, understanding the decadal variability of the ITF requires a multidecadal time series of ITF. Such long-time observations of the ITF volume transport can be extracted from the frequently repeated expendable bathythermograph (XBT) section between Western Australia and Java – the IX01 line.

This XBT volume transport data is available from 1983. Apart from observations, numerical models' sophistication and refinement have allowed the study of ITF using general circulation models or regional ocean models. The mean ITF volume transport from these models is between 12-17 Sverdrup, consistent with the observations (Metzger et al. 2010; Potemra. 2005; Tozuka et al. 2009). To achieve the objectives of the current Chapter 2, SSH data from different sources were used - the Archiving, Validation, and Interpretation of Satellite Oceanography (AVISO) satellite observed SSH data from the year 1993 to 2015, ORAS4 reanalysis data for SSH, and ITF volume transport calculation for 1959 to 2015, and ORA-S3 reanalysis data for surface wind stress during 1959-2009.

AVISO offers a high-resolution gridded dataset created from different satellite altimetry measurements, namely, TOPEX/Poseidon, ERS-1 & 2, Jason-1, 2 & 3, SARAL/AltiKa, Envisat and Cryosat-2. In this study, monthly data on a $1^{o}\times1^{o}$ grid spanning from 1993 to 2015 was used.

The ORAS4 dataset provides global ocean reanalysis monthly mean data prepared by the European Centre for Medium-Range Weather Forecasts (ECMWF) ocean analysis-reanalysis system. ORAS4 reanalysis uses the Nucleus for European Modelling of the Ocean (NEMO) model (Madec, 2008) and ocean data assimilation system developed by (Mogensen et al., 2012) - variational assimilation system NEMOVAR. The analysis cycle in ORAS4 is 10 days; every 10 days the NEMO model is integrated forward forced by daily surface fluxes and relaxed sea surface temperature.

The ocean model is forced by atmospheric-derived daily surface fluxes, instead of being computed using a bulk formula within NEMO. Daily fluxes of solar radiation, total heat flux, evaporation-minus-precipitation and surface wind stress are taken from the ERA-40 reanalysis (Uppala et al., 2005) from September 1957 to December 1989, ERAInterim reanalysis (Dee et al., 2011) from January 1989 to December 2009, and the ECMWF operational archive from January 2010 onwards.

### 2.2.1 Inter-comparison of ITF volume transport based on ORAS4 reanalysis data and in-situ observations

The observed and reanalysis dataset is used to estimate the ITF volume transport in the current chapter. Observed volume transport through the Makassar Strait inflow passage accounts for 80% of the total ITF transport, thus a good proxy for the total ITF transport (Gordon et al. 2008). The ITF volume transport outflow can also be extracted by integrating

**Figure 2.1**: Typical Indonesian Throughflow transport geography.

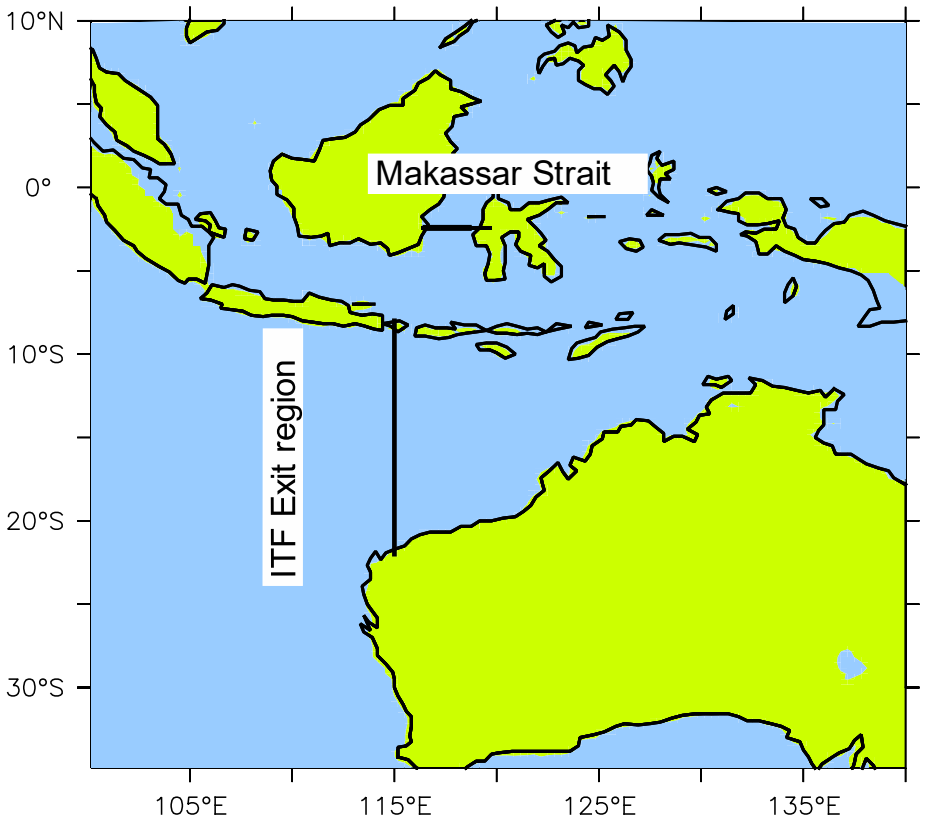

zonal velocity from the surface to the bottom near the IX01 line. Hence, the monthly mean long-term variability in the volume transport of the ITF from 1959 to 2015 is calculated at 2 locations, as indicated by black line in the Figure 2.2. First in Makassar Strait, integrated from surface to 1000 m depth and between 116.5$^{o}$E and 120.0$^{o}$E at 3.5$^{o}$S, and the second along the IX01 (115$^{o}$E) line, from surface to bottom between 9$^{o}$S to 20$^{o}$S, based on the Ocean Reanalysis System 4 (ORAS4) dataset (Balmaseda et al. 2013).

ORAS4 data shows an average transport of ~13.1 Sv and ~13.8 Sv in Makassar strait and along the IX01 line, respectively, from the Pacific Ocean to the Indian Ocean during the 2004 to 2011 period, comparable to the observational mean value (~12.6 Sv) for the same period (Gordon et al. 2012). While the mean observed volume transport in the Makassar Strait during 2014 and 2015 was 11.5 and 9.8 Sv, respectively (Li et al. 2018), the ORAS4 data also shows similar results with 11.1 (11.6) Sv transport in 2014 and 9.1 (9.5) Sv in 2015 within Makassar Strait (along the IX01 line). Although the period for the inter-comparison is minimal, the intercomparison of ITF volume transport based on the direct measurements and ORAS4 reanalysis data indicate that the ORAS4 can represent the interannual and decadal variability of the ITF.

**Table 2.1**: Observational and reanalysis ITF volume transport in different Makassar Strait and along the IX01 line in Indian Ocean (Gordon et al. 2012, Li et al. 2018)

| Year | Inflow passages in Pacific Ocean | Outflow passages in Indian Ocean |
|---|---|---|
| | Makassar Strait | Along IX01 line |
| 2004-2011 | 13.1 Sv | 13.8 Sv |
| 2014 | 11.5 Sv | 11.1 Sv |
| 2015 | 9.8 Sv | 9.1 Sv |

## 2.3 Results

### 2.3.1 Decadal ITF transport based on assimilated velocity and SSH difference in the ORAS4

To capture the decadal variability of the ITF 85-months running mean was applied to the ITF transport based on the velocity simulated in the ORAS4 reanalysis dataset (Figure 2.3). The variability of the ITF at both locations, calculated at Makassar Strait and ITF exit region, is same with little systematic bias. These time series again confirms that the ORAS4 reanalysis can capture the inflow and outflow of ITF to a good extent. Hence, onwards only the ITF transport based on the Makassar Strait is used for analysis.

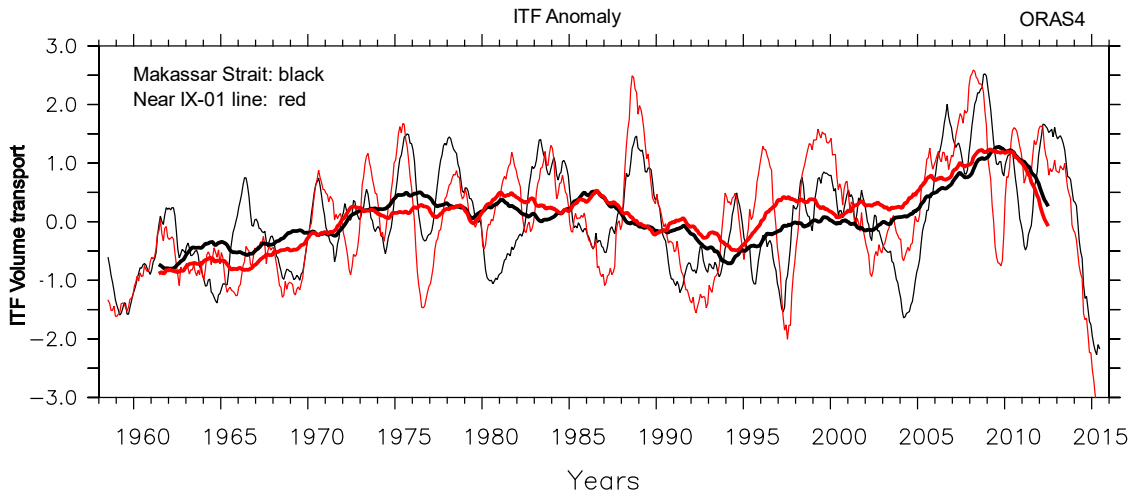


**Figure 2.2** Time series of the ITF volume transport in Makassar Strait (black curve) and near IX01 line (red curve) (1 Sv=10 $m^6$ $s^{-1}$) based on the ORAS4. The transport is calculated by vertically integrating the monthly mean velocity from the surface to 1000-meter depth in Makassar Strait and the surface to the depth above the bottom from Australia to Indonesia between 9°S and 20°S along 115°E (near IX01). A 13-month (85-month) running mean was applied on the thin curve (thick curve).

Correlation and regression analysis is a widely accepted method for understanding the relationship between two or more variables. The correlation (Figure 2.3a) and regression (Figure 2.3b) coefficients between the vertically integrated meridional velocity and SSHA variations on a decadal timescale were calculated using the ORAS4 dataset for the 1959-2015 period to identify if it is still a good indicator in representing the decadal ITF variations. Before that, area-averaged Indo-Pacific SSH (65$^{o}$E to 165$^{o}$E, 20$^{o}$S to 20$^{o}$N) is subtracted from the SSH all over the globe. Correlation and regression analyses between sea level and ITF transport reveal the oceanic regions that affect ITF variability on a decadal timescale. A pair of significant positive correlation and regression coefficients in the NWP region and negative ones in the SEI region are associated with the enhanced ITF transport, vice versa, showing that Wyrtki's theory can be applied to the decadal time scales.

A significant positive correlation is observed in the western north Pacific Ocean, with the correlation coefficient (R) reaching as high as 0.9 in a small region. The high correlation in the NWP region indicates, higher sea surface height in this region funnels more ITF volume through the Indonesian islands. The region of high correlation in the NWP region (125-155$^{o}$E, 6-16$^{o}$N) with the ITF transport was selected as a region that affects the ITF variability significantly.

The negative correlation is observed in the SEI region. A significantly high correlation is observed in the east equatorial Indian Ocean (EEIO) with the ITF variability on a decadal timescale. The correlation value reached as high as 0.8 in the EEIO [5$^{o}$S–5$^{o}$N, 65–95$^{o}$E]. However, the conventional ITF exit region in the Indian Ocean was also selected to calculate the inter-ocean SSH gradient [85–115$^{o}$E, 6-16$^{o}$S] between the Pacific and Indian Oceans since that region shows significantly high regression values.

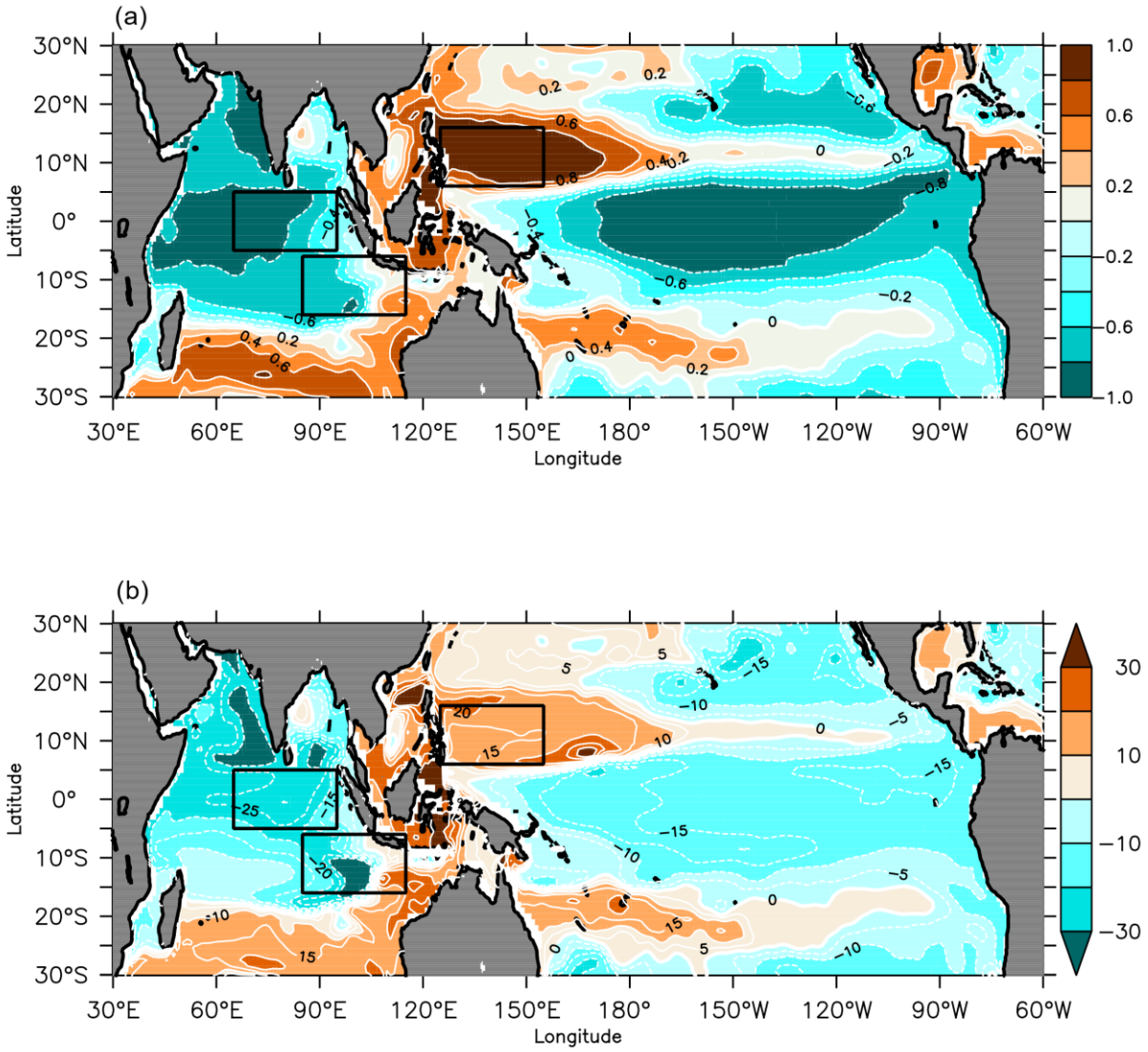


**Figure 2.3** (a) A map of correlation coefficients (contoured for every 0.2) in the decadal SSHA onto the decadal volume transport variation near IX01 line as in Fig. 2.1. The coloring convention is shown on the right of the panel. Regions in the inset black rectangles are the NWP (6–16°N, 125–155°E), EEIO (5°S–5°N, 65–95°E), and SEI (6–16°S, 85–115°E) regions selected for the calculation of the SSHA difference. (b) as in (a) but for regression coefficient (contoured for every 10 cm/Sv).

The selected regions are represented as the inset black rectangles in Figure 2.3. The SSHA variations in these three regions based on the ORAS4 and AVISO are identical during 1993–2015 (Figure 2.4), although there is a slight systematic bias in the mean values.

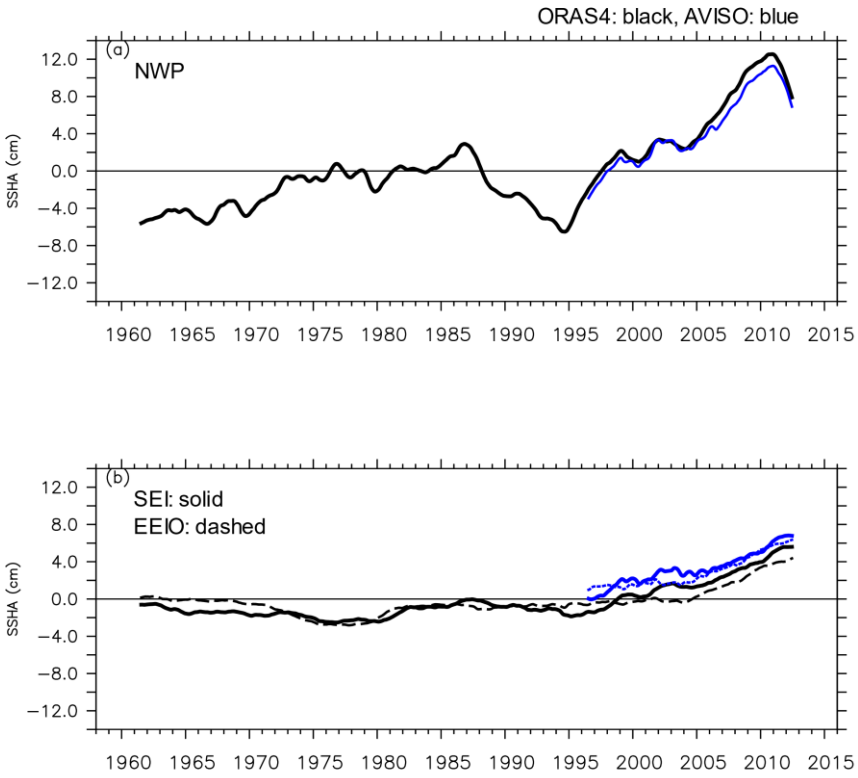


**Figure 2.4** (a) Time series of the decadal SSHA (cm) over the NWP region based on the ORAS4 (thick black curve) and AVISO (blue curve). (b) As in (a), but for the SEI region (solid curves) and the EEIO region (dashed curves).

This confirms that the reanalysis data has good skill in reproducing the SSHA variations observed by the satellites. However, the assimilation for the reanalysis involves most of the observed data, including the AVISO SSHA. Although the decadal ITF transport negatively correlates with the SSHA over the EEIO region than in the SEI region, Figure 2.3b shows the SEI region has higher skill in estimating ITF variability on the decadal time scale. Figure 2.5 confirms that the SSHA difference between the NWP and SEI regions is highly correlated with the decadal ITF volume transport (correlation coefficient, R=0.95) than the SSHA difference between the NWP and EEIO (R=0.93). Therefore, the SEI region as the ITF exit region in calculating the SSHA difference is selected in the following parts.

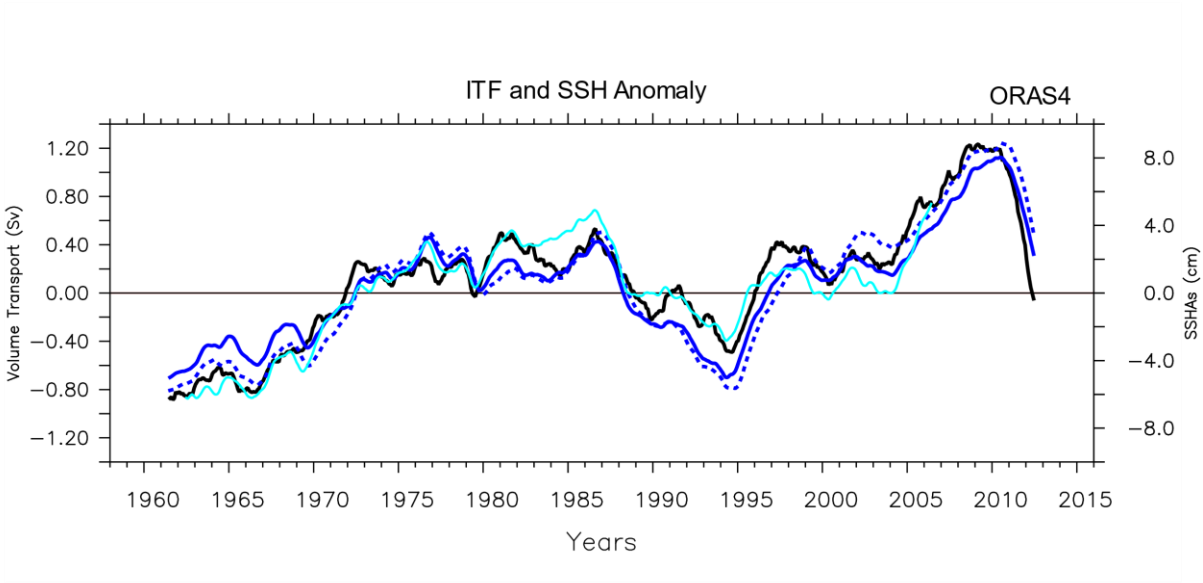


**Figure 2.5** Time series of the decadal ITF transport anomalies (Sv, black line) and the SSHA difference (cm) across the NWP–SEI regions (blue solid curve), and across the NWP–EEIO regions (blue dashed curve) based on the ORAS4 reanalysis. The estimated SSHA difference across the NWP–SEI regions are also superimposed (light blue solid curve). The axis for the ITF transport is on the panel's left side, and the SSHA difference's axis is on the right.

### 2.3.2 Decadal ITF transport based on the direct SSHA difference

As discussed in previous section, the SSHA difference across the Indonesian Archipelago is a good indicator of ITF variations on the annual and interannual time scales. In the entrance and exit regions of the ITF, the SSHA is significantly correlated with the ITF variations. Hence, the NWP [6–16°N, 125–155°E] and SEI [6–16°S, 85–115°E] regions are selected for calculating the SSHA difference as a proxy index of the ITF variability. In addition to the SEI region, the EEIO region (5°S–5°N, 65–95°E) is selected to calculate the SSHA differences.

The decadal ITF variability is negatively correlated with the SSHAs in the EEIO and SEI regions. However, Figure 2.5 shows that the SSHA difference between the NWP and SEI regions is slightly well correlated with the decadal ITF volume transport (correlation

coefficient, R=0.95) than the SSHA difference between the NWP and EEIO (R=0.93). Therefore, the SEI region was selected as the exit region to calculate the SSHA difference in the later sections. Following Wyrtki's (1987) idea, the SSHA difference was linearly regressed onto the ITF variation. The resulting linear regression relation is expressed as follows,

$$\textit{ITF anomaly [Sv]} = 0.185\ [\text{Sv cm}^{-1}] \times \textit{SSHA Difference [cm]} + 0.002\ [\text{Sv}]$$

### 2.3.3 Decadal ITF transport based on estimated SSHA difference

Besides using the direct SSHA as an output variable in the reanalysis data sets, the estimated SSHA fields are calculated using a 1.5-layer reduced gravity model forced by wind stress with the boundary condition along the coast to the east. This method for estimating the SSHA difference using only atmospheric data has a substantial advantage in overcoming the challenges of lower spatial resolution in the ocean component of the CMIP5 models. The previous studies (Abe et al. 2014; Vivier et al. 1999; Watanabe and Ilson 2016) confirm that the reduced gravity model can reproduce observed SSHAs, including the feature of the westward propagating Rossby waves indicated by the satellite measurements over the tropical Pacific, in this study, the same model was utilized as in Abe et al. (2014).

This 1.5-reduced gravity model has successfully reproduced the wave feature in several studies and proved to be very effective along with Abe et al (2014) (e.g., Meyers 1979; Kessler 1990; Fu and Qiu 2002; Capotondi et al. 2003; Qiu and Chen 2010). A linear vorticity equation is obtained under the long wave approximation.

$$\frac{\partial h'}{\partial t} - C_R \frac{\partial h'}{\partial x} = -\frac{g'}{\rho_0 g}\mathbf{k} \cdot \nabla \times (\tau'/f) - \varepsilon h'$$

Where $h'$ is the SSHA, $\tau'$ is the wind stress anomaly vector, $C_R$ is the propagation speed of the long baroclinic Rossby waves, g' is the reduced gravity, $\rho_0$ is the reference density, $f$ is the

Coriolis parameter, $k$ is a unit vector normal to the x–y plane, and $\varepsilon$ is the dissipation ratio. The parameters $C_R$ and $f$ changes with the latitude. The $C_R$ was decided empirically and the $f$ based on the Coriolis Force equation. The monthly averaged wind stress anomaly provided by the ORA-S3 reanalysis are used to calculate the estimated SSHA. The wind force was zonally integrated along the 6-16$^o$N latitude in the Pacific Ocean and 6-16$^o$S latitude in the Indian Ocean.

The surface wind stress from the ORA-S3 ocean reanalysis forcing was used for estimating the SSHA with the 1.5-layer reduced gravity model. The ORA-S3 uses Hamburg Ocean Primitive Equation model (HOPE) after several modifications (Wolff et al. 1997; Anderson and Balmaseda 2005). Similar to the ORAS4, ORA-S3 is forced with daily fluxes of solar radiation, total heat flux, evaporation-minus-precipitation and surface wind stress are taken from the ERA-40 reanalysis (Uppala et al., 2005) from September 1957 to December 1989, ERAInterim reanalysis (Dee et al., 2011) from January 1989 to December 2009. However, the ORA-S3 reanalysis also provides a wind forcings data as well along with the oceanic reanalysis data. Using this wind stress dataset, the estimated SSHA were obtained with the 1.5-reduced gravity model.

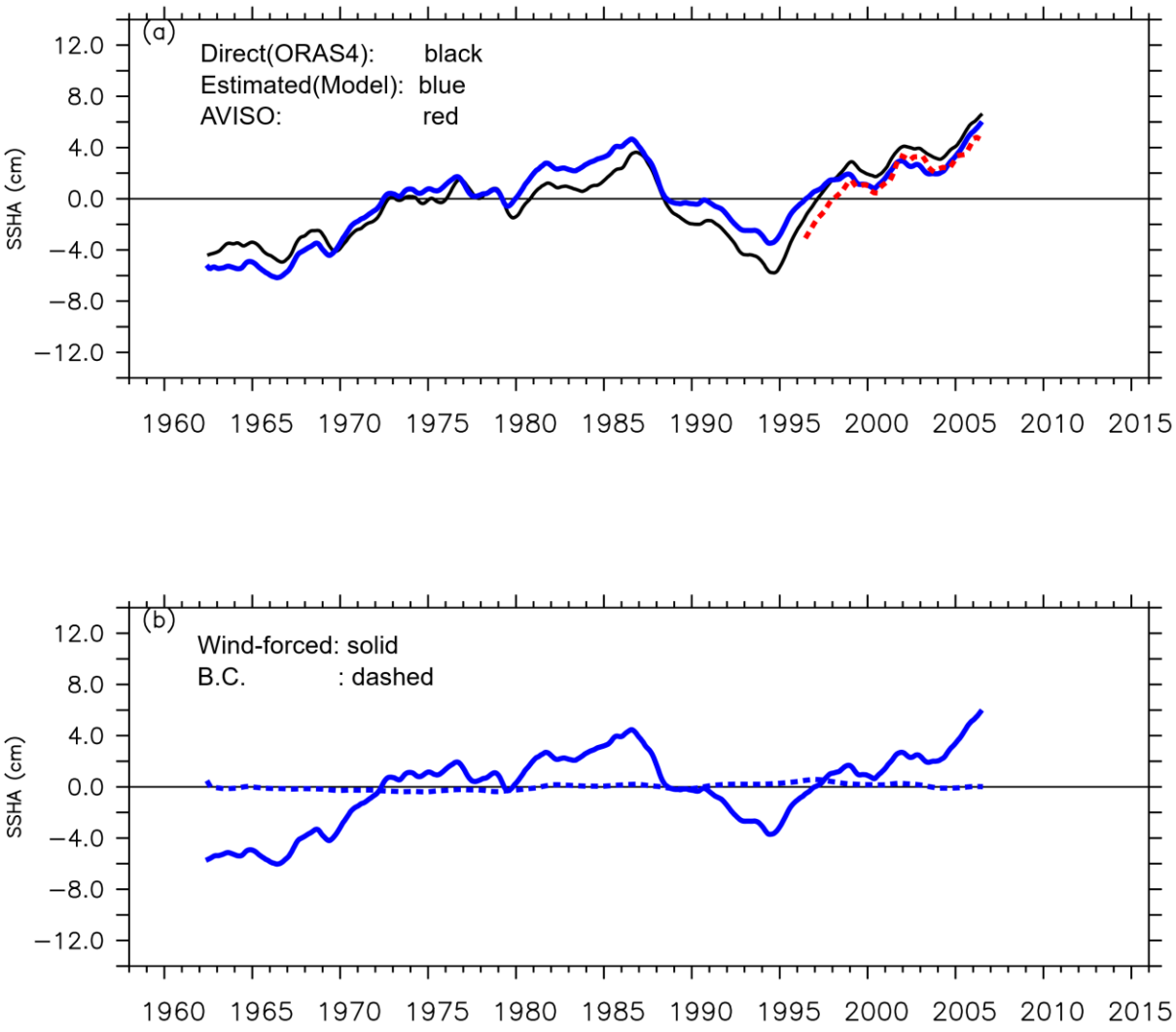


**Figure 2.6** (a) Time series of the decadal SSHA (cm) in the NWP region based on the ORAS4 ("direct" SSHA by black curve), reduced gravity model forced by the ORA-S3 wind stress curl ("estimated" SSHA by blue curve), and AVISO (red dashed curve). (b) as in (a), but for the wind-forced component (blue thick curve) and the boundary condition component (blue dashed curve) in the estimated SSHA.

To reproduce the SSHA in the NWP region (6–16°N, 125–155°E), the 1.5-layer reduced gravity model was forced by the monthly wind stress anomaly all over the Pacific Ocean basin with the boundary condition along the eastern coast in the 6–16°N latitude band. Our inter-

comparison of the SSHAs with the satellite observation and direct output of the ORAS4 shows that the decadal SSH variations of the NWP region are successfully reproduced in the reduced gravity model (Fig. 2.6a). Owing to the long distance of the wave propagation toward the NWP region, the boundary condition along the eastern coast has no substantial effect on the estimated SSHA in the NWP region (Fig. 2.6b). This means that the SSHAs in the NWP region can be estimated without the coastal boundary condition as the ocean component output.

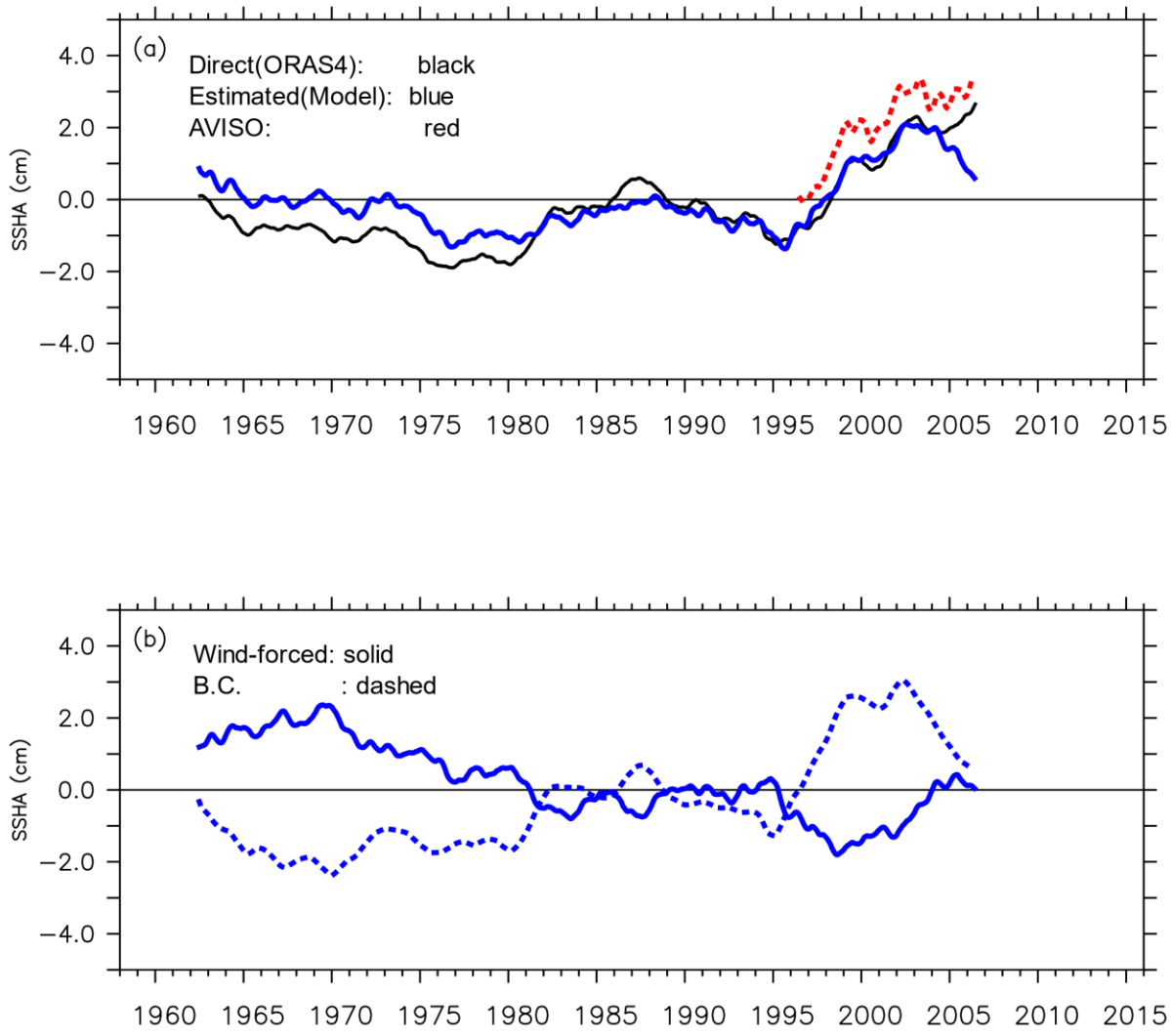


**Figure 2.7** As in Fig. 2.6, but for the SEI region.

By contrast, the SEI region is close to the coastal boundary. Therefore, it is expected to require the wind stress curl and the boundary condition better to estimate the SSHA by the reduced gravity model. As expected, both the wind forcing and the boundary condition contribute to reproducing the observed SSHA in the SEI region (Fig. 2.7a), while the contribution from either of those is unable to reproduce it (Fig 2.7b).

However, our intention for the estimated SSH is to seek the appropriate procedure without beforehand using the SSH information for the calculations of the reduced gravity model. Schouten et al. (2002) show that an eastward Kelvin wave forced by the equatorial zonal wind stress over the Indian Ocean controls the SSH variations along the eastern coast in the SEI region. Indeed, the SSH variations of the SEI region are significantly correlated with the zonal wind stress anomalies over the central portion of the equatorial Indian Ocean (5°N–10°S, 65–105°E) (Fig. 2.8).

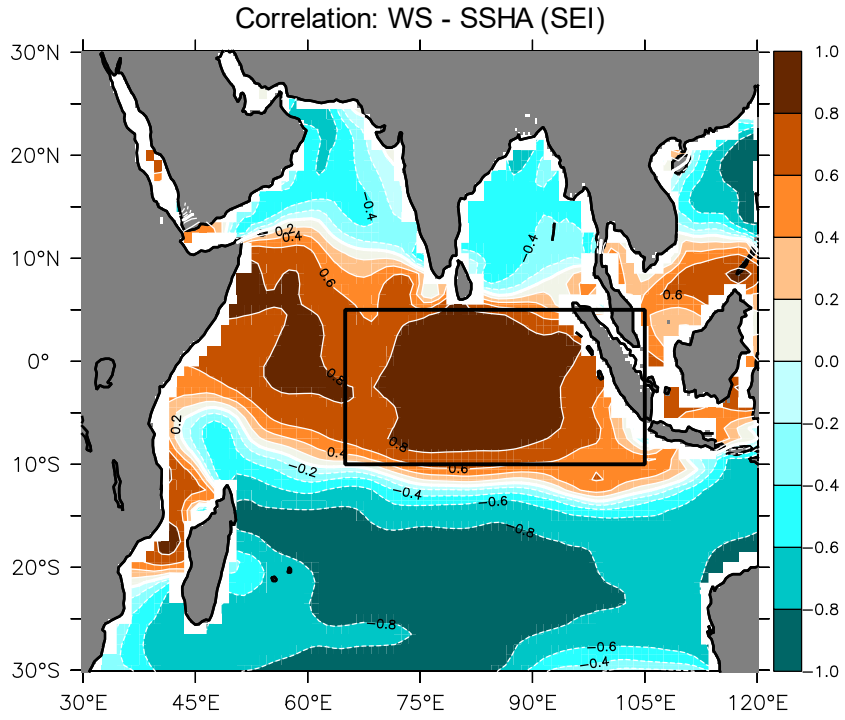


**Figure 2.8** A map of correlation coefficients on a decadal timescale (contoured for every 0.2) in zonal wind stress anomalies in ORA-S3 onto the effect of boundary condition SSHAs averaged over the SEI region based on the ORAS4. The coloring convention is shown on the right of the panel.

Hence rather than using the boundary condition directly from the satellite observation and/or reanalysis data set, a regression analysis based on the equatorial zonal wind-stress is used in calculating the contribution of the boundary condition to the SSHA in the SEI region as follows,

$$h_b(SEI)\ [cm] = \tau_x[Pa] \times 425\ [cm\ Pa^{-1}] - 0.342\ [cm],$$

where $h_b$ (black curve of Fig. 2.9) is a contribution of the coastal boundary condition onto the estimated SSHA in the SEI region, and $\tau_x$ is 85-month running mean anomalies of zonal wind stress over the central portion (5°N–10°S, 65–105°E) of the Indian Ocean.

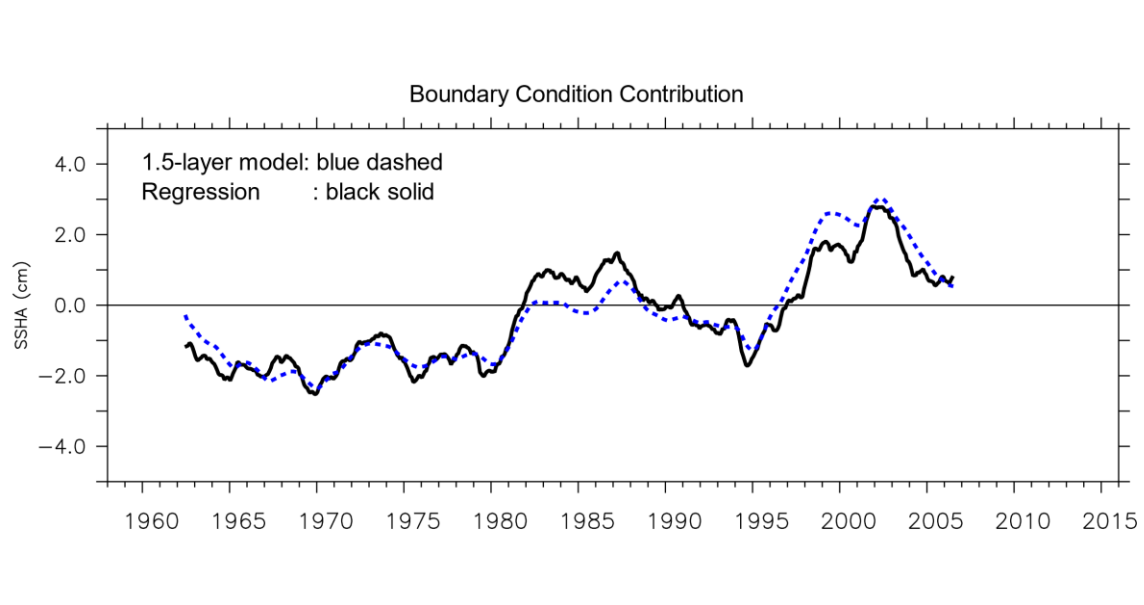


**Figure 2.9** Time series of the boundary condition component (blue dashed curve) in the estimated SSHA by the reduced gravity model (same as in Fig. 2.8b) and the calculated boundary condition contribution to the SSHA in the SEI region using a regression analysis with the equatorial (5°N–10°S, 65–105°E) zonal wind stress of the ORA-S3 (solid black curve).

Consequently, there is a two-step procedure to earn the estimated SSHA in the SEI region. First, the wind forced component is calculated by the reduced gravity model. Then, in the second step, the contribution of the coastal boundary condition from the surface wind

anomalies using the regression analysis is added to the wind forced component. Our inter-comparison shows that the estimated SSH by this two-step procedure is mostly identical to the direct SSHA (Figure 2.7a).

As the usage of the direct SSHA is discussed in Section 2.3.2, the differences in the estimated SSHA between the NWP and SEI regions are utilized to represent the ITF variations. Figure 2.5 compares the meridional volume transport within Makassar Strait in the ORAS4 reanalysis data with the direct and estimated SSHA differences between the NWP and SEI regions. The significant correlation coefficients among those time series show that the estimated SSHA proposed in this subsection is useful to represent the decadal variations in the ITF volume transport only based on the atmospheric variable. Hence, as documented in the later sections, the same procedure was applied to the CMIP5 data set.

## 2.4 Summary and discussion

The longest continuous observations of the ITF volume transport are available only from 2004 to 2011. These observations are not long enough for the analysis of the ITF on decadal timescale. Comparison of the available observations and the ORAS4 reanalysis dataset show that the reanalysis data has a good skill in capturing the ITF variability in both the inflow and outflow regions of the ITF. Hence, the multidecadal timeseries of ITF volume transport was obtained with the ORAS4 reanalysis dataset. Further the correlation and regression analysis between ITF and SSHA on decadal timescale show that the SSH difference between the NWP and SEI regions can capture the ITF variability with correlation exceeding 0.9, indicating that the SSH difference can be used to track the ITF variability very well.

Besides using direct SSHA difference to capture the ITF variability, we also devised a

new method of tracking the ITF variability with only surface wind dataset. For this purpose, a 1.5-layer reduced gravity model was forced with the wind stress to estimate the SSHA over the NWP and SEI regions. SSHA estimation over the NWP region with the 1.5-layer reduced gravity model is straight forward, however the SSHA estimation over the SEI region is slightly complicated. The SSHA due to boundary condition propagating westward also has significant variation in SEI region. The correlation analysis reveals that the central equatorial zonal wind stress can track the variability of SSHA due to boundary condition very well. Hence, the regression technique was used to estimate the SSHA due to boundary condition. Consequently, two step procedure was followed to estimate the SSHA in the SEI region as explained in the previous section.

Significant correlation was obtained among the ITF volume transport calculated with different methods. Hence, the same procedure of tracking the ITF variability with the estimated SSHA was used for CMIP5 dataset in later sections.

# Chapter 3: CMIP5 model diagnosis and selection in the historical simulation

## 3.1 Introduction

One of this study's objectives is to understand future changes in the relative contribution of the Pacific and Indian Oceans to decadal ITF variation. For this purpose, the Coupled Model Intercomparison Project - 5 (CMIP5) historical and RCP8.5 scenario simulations were used as the current and future climate realizations, respectively. CMIP5 is a framework for ocean-atmosphere general circulation models to understand climatic processes and provides probabilistic estimates of future climate change. However, the climate model simulations for the purpose of this study are challenging because model reproducibility of the ocean components in the marginal seas, including the SSH variations around the Indonesian Archipelago, is not always guaranteed, primarily due to insufficient horizontal resolution and associated unrealistic bottom topography. Hence, this chapter aims to select the appropriate models for analyzing decadal ITF variations. For this purpose, different metrics were used to select appropriate CMIP5 models.

The ITF variability is controlled by the SSH difference between the NWP and SEI regions. Since the CMIP5 models' coarse resolution sometimes fails to resolve Makassar Strait, hence the correct representation of ITF volume transport in that strait is not always guaranteed. Hence, the CMIP5 models were analyzed to check if they have a good skill in reproducing the SSH difference between NWP and SEI regions. The historical simulations were compared to the observations for the 1959-2005 period. One of the metrics for model selection is based on the climatological mean SSH difference between the NWP and SEI regions. An attempt was made to shortlist the CMIP5 models that show comparable climatological mean SSH

differences between NWP and SEI regions to the observed data.

Since the discrepancy was found in the SSHA variability among the models, the reproducibility of the direct SSHA with the estimated SSHA was compared with the reanalysis. With an advantage of the estimated SSHA, forced only by wind stress data, an inter-comparison of the direct and estimated SSHA differences between the NWP and SEI regions was made (Figure 3.1). As stated in the following parts of this section, thirteen (13) CMIP5 models are retained, screened by the mean SSH difference within a range of one standard deviation (10.7–22.6 cm) of multi-model spread. Multimodal mean SSHA of these 13 models will be used to compare the Indo-Pacific region's contribution to the decadal variation of the ITF.

## 3.2 Data and Analysis methods

A direct SSH data from the 23 CMIP5 models for the period of 47 years between 1959-2005 from historical simulation and ensemble r1i1p1, as listed in Table 3.1, was used to calculate the climatological mean SSH difference between NWP and SEI regions. The climatological mean of the SSH over the NWP and SEI regions was calculated by averaging the region defined in section 2.3. The mean SSH difference in these CMIP5 models was then compared with the mean SSH difference in the ORAS4 (Balmaseda et al., 2013) reanalysis dataset to evaluate its reproducibility in the CMIP5 models.

The surface wind-stress variables for the same period (1959-2005) from the historical simulation and the r1i1p1 ensemble from the 23 CMIP5 models are used. The wind stress data was utilized to calculate the estimated SSHA and make the inter-comparison of the direct and estimated SSHA in the selected regions.

**Table 3.1** CMIP5 dataset variables used for the analysis

| CMIP5 variable | Simulation | Ensemble | Year |
|---|---|---|---|
| **SSH** | Historical | r1i1p1 | 1959-2005 |
| **Zonal & Meridional component of surface wind stress** | Historical | r1i1p1 | 1959-2005 |

## 3.3 CMIP5 model diagnosis and selection

Most CMIP5 models cannot resolve the Indonesian islands; thus, the ITF volume transport calculation with the velocity field in the Makassar strait is often impossible in the CMIP5 models. Instead, the well-understood relationship between the ITF variation and the SSH difference between the NWP and SEI regions was utilized to calculate the ITF volume transport and diagnose the CMIP5 models. The mean SSH difference between the NWP and SEI regions was used as a metric for CMIP5 model selection. As listed in Table 3.1, there is a large inter-model spread in reproducing the mean SSH difference among the 23 CMIP5 models. While 21 models represented a downward SSH gradient from the Pacific to the Indian oceans, which can represent realistic ITF flow from the Pacific towards the Indian Ocean, the other two showed an upward gradient.

Among 23 CMIP5 models, the INM-CM4 and CanESM2 models showed the upward mean SSH gradient, -18.54cm and -12.93, respectively. This upward gradient suggests the opposite mean flow from the Indian Ocean towards the Pacific Ocean, which is unrealistic. The climatological mean SSH value estimated in the Indian Ocean is much higher in both models compared to other oceanic regions. Hence, both models showed an upward SSH gradient and were rejected from further analysis.

**Table 3.2** Climatological mean SSH difference between the NWP and SEI regions of the individual CMIP5 models, along with the horizontal resolutions of the atmospheric and ocean model components around those two regions for the individual models. Rows 6–18 with the bold fonts indicate the employed 13 models, where the simulated SSH difference is within the one standard deviation of the inter-model spread. See the body text for details regarding the calculation of the inter-model spread.

| | Model | Climatological Mean SSH Difference (cm) | Horizontal resolution of atmospheric model component | | Horizontal resolution of ocean model component | |
|---|---|---|---|---|---|---|
| | | | Latitude ($^{O}$) | Longitude ($^{O}$) | Latitude ($^{O}$) | Longitude ($^{O}$) |
| 1 | INM-CM4 | -18.54 | 1.50 | 2.00 | 0.50 | 1.00 |
| 2 | CanESM2 | -12.93 | 2.79 | 2.81 | 0.93 | 1.40 |
| 3 | MPI-ESM-LR | 5.21 | 1.86 | 1.87 | 0.80 | 1.40 |
| 4 | NorESM1-ME | 9.39 | 1.89 | 2.50 | 0.54 | 1.13 |
| 5 | NorESM1-M | 10.50 | 1.89 | 2.50 | 0.54 | 1.13 |
| **6** | **MRI-CGCM3** | **11.59** | 1.12 | 1.12 | 0.50 | 1.00 |
| **7** | **MRI-ESM1** | **11.81** | 1.12 | 1.12 | 0.50 | 1.00 |
| **8** | **IPSL-CM5A-MR** | **12.45** | 1.26 | 2.50 | 1.98 | 1.30 |
| **9** | **MIROC5** | **12.58** | 1.40 | 1.40 | 0.80 | 1.40 |
| **10** | **IPSL-CM5A-LR** | **12.61** | 1.89 | 3.75 | 1.30 | 1.98 |
| **11** | **GFDL-CM3** | **13.18** | 2.00 | 2.50 | 1.00 | 1.00 |
| **12** | **CCSM4** | **13.54** | 0.94 | 1.25 | 1.11 | 0.54 |
| **13** | **GFDL-ESM2M** | **14.50** | 2.02 | 2.50 | 1.00 | 1.00 |
| **14** | **MPI-ESM-MR** | **14.75** | 1.86 | 1.87 | 1.87 | 1.87 |
| **15** | **GFDL-ESM2G** | **16.40** | 2.02 | 2.00 | 1.00 | 1.00 |
| | **ORAS4** | **18.40** | | | 0.30 | 1.00 |
| **16** | **CMCC-CMS** | **21.08** | 3.71 | 3.75 | 2.00 | 2.00 |
| **17** | **IPSL-CM5B-LR** | **21.63** | 1.89 | 3.75 | 1.30 | 1.98 |
| **18** | **CMCC-CM** | **21.86** | 0.74 | 0.75 | 2.00 | 2.00 |
| 19 | HadGEM2-ES | 23.03 | 1.25 | 1.87 | 1.00 | 1.00 |
| 20 | HadGEM2-CC | 24.13 | 1.25 | 1.87 | 1.00 | 1.00 |
| 21 | ACCESS1-3 | 24.53 | 1.25 | 1.87 | 1.00 | 1.00 |
| 22 | CSIRO-Mk3-6-0 | 26.34 | 1.86 | 1.87 | 0.93 | 1.87 |
| 23 | ACCESS1-0 | 26.75 | 1.25 | 1.87 | 1.00 | 1.00 |
| | Ensemble mean | 13.85±10.8 | | | | |

Using 21 models with a realistic downward gradient, a multi-model ensemble mean value of SSH difference is 16.7 cm, which is close to the observed mean SSH difference (18.4 cm). However, the mean SSH difference ranges from 5.21 to 26.75, indicating a large inter-model spread. Hence, only CMIP5 models within one standard deviation of the inter-model spread were selected for further analysis.

While most of the 23 CMIP5 models show (Figure 3.1 & Figure 3.2) similar ITF variation on decadal timescale, very few models (only 3) with low correlation (R >= 0.6) between direct and estimated SSHA show a significantly different variation in SSHA difference. CanESM2, MPI-ESM-LR, and NorESM1-ME models show a correlation value of less than 0.6 between direct and estimated SSHA variation. The selected thirteen (13) CMIP5 models screened by the mean SSH difference in a range of one standard deviation (10.7-22.6) to the multi-model ensemble mean show the same variation in direct and estimated SSHAs. The same variation in both types of SSHA also indicates that atmospheric winds drive the variability of the SSHA over these regions. Figure 3.1 shows the time series on the decadal timescale of the SSHA differences between NWP and SEI regions using both direct (black time series) and estimated (red time series) SSHAs from selected (13) CMIP5 models. Figure 3.2 shows the time series on the decadal timescale of the SSHA difference of unselected models.

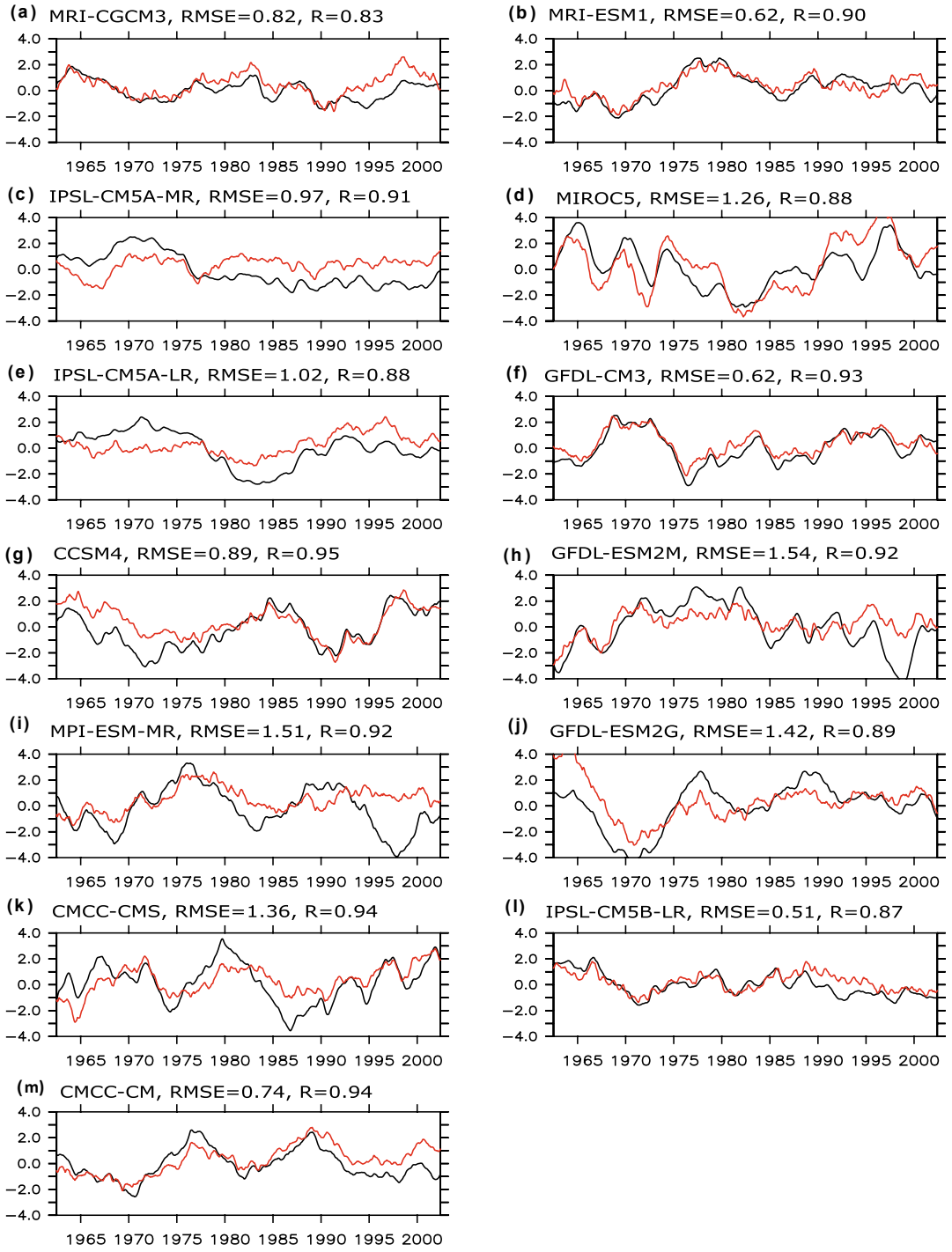


**Figure 3.1:** Time series of the decadal SSHA difference (cm) across the NWP–SEI regions, based on the simulated direct SSHA in the selected CMIP5 models (black curve) and the estimated SSHA (red curve) by using the simulated wind stress of those models. Simultaneous correlation coefficients between those direct and estimated SSHAs are indicated on each panel's upper right corner.

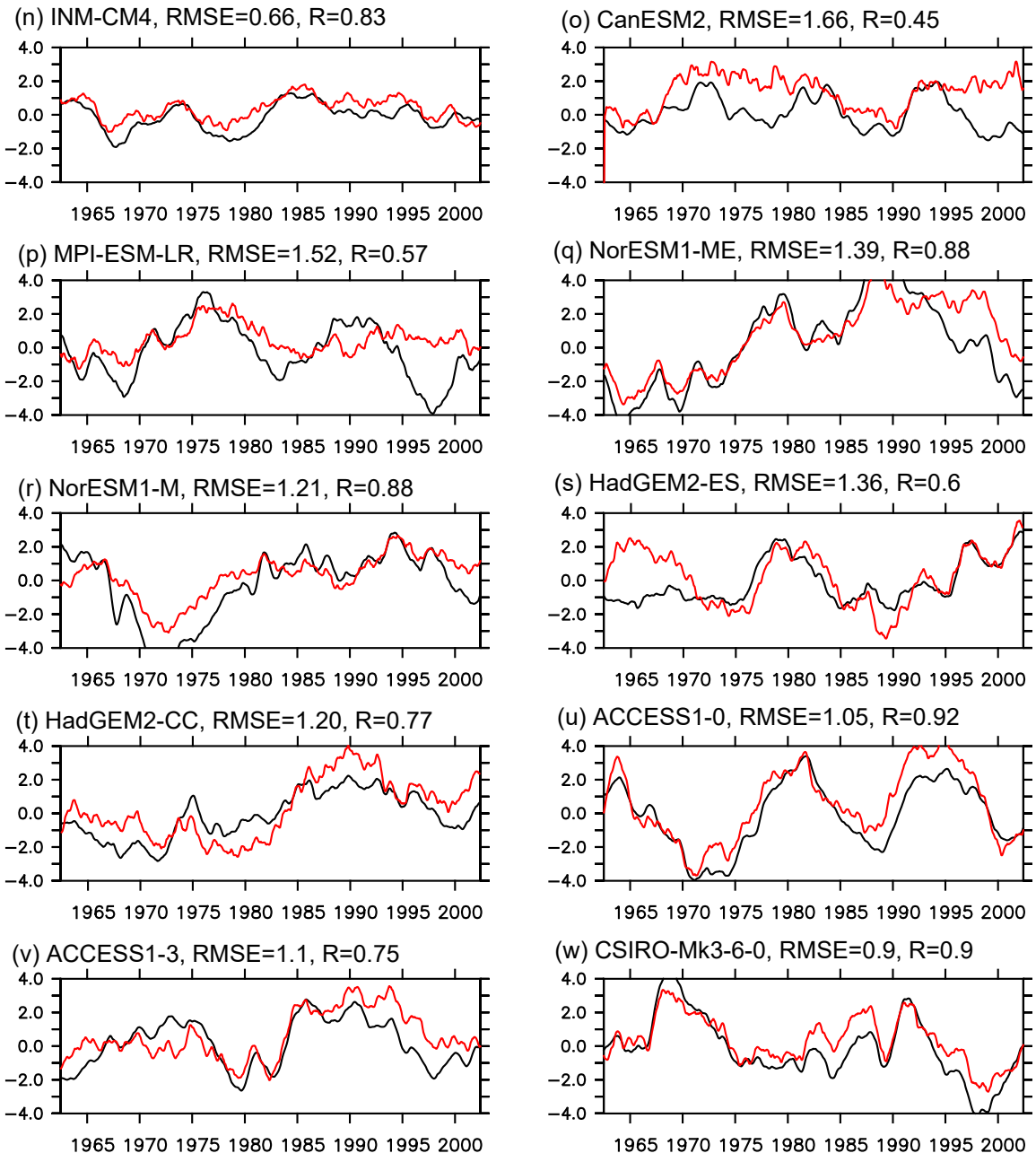


**Figure 3.2:** Same as Fig. 3.1 but for not-selected CMIP5 models.

## 3.4 Summary and discussion

Understanding the future changes in the relative contribution from the Pacific and Indian Oceans to the decadal variation of the ITF is one of the study's main objectives. To achieve the objectives, the CMIP5 RCP8.5 climate scenario for future projections and historical simulations were utilized to compare the future projections with the historical climate. However, most CMIP5 models have a coarse resolution, and the reproducibility of the ocean components is not always guaranteed in these coarse-resolution models. Such CMIP5 models cannot resolve Indonesian Archipelago; hence, the ITF volume transport calculation is often impossible with the Makassar Strait's velocity field. Hence not all the models can be used as-is for our research objectives. Also, ITF volume transport calculation is difficult in the different inflow and outflow passages. Hence, the newly developed method of ITF estimation with the SSH difference is employed for CMIP5 model diagnosis and selecting the only models that pass the selection metrics.

The inter-comparison of the direct and estimated SSHA difference of the CMIP5 models was conducted to check for any discrepancy. While most of the CMIP5 models shows the variation in the direct and estimated SSHA is mostly identical, some of the models show different variation, indicating the difference in the ITF estimation within the model. Only 13 of the 23 CMIP5 models passed the selection criteria based on the climatological mean SSH difference and the direct and estimated SSHA difference covariance comparison. Hence, only 13 CMIP5 models were retained to analyse the relative contribution from the Pacific and Indian Ocean to ITF variation on a decadal timescale.

# Chapter 4: Contribution of the Pacific and Indian Oceans to the decadal variation of Indonesian throughflow in historical simulation and RCP8.5 scenario.

## 4.1 Introduction

It is widely accepted from the model studies (Murtugudde et al. 1998; Vranes et al. 2002; Lee et al. 2015) that the Indonesian Throughflow transfers a significant amount of the heat from the Pacific to the Indian Ocean and plays a vital role in modulating the climate of Indian Ocean rim countries and ENSO dynamics with a delayed response. Previous studies have identified how the Indian and Pacific Oceans contribute to the ITF's seasonal, interannual, and decadal variability (Masumoto 2002; Drushka et al. 2010; Sprintall and Revelard 2014; Wyrtki 1987). These studies pointed out that the Indian Ocean and the Pacific Ocean SSH are equally important to the ITF variation on the seasonal and interannual timescale. Murtugudde et al. (1998) showed that if the interannual variation of the Indian Ocean is removed from the ITF, the correlation between the Southern Oscillation Index (SOI) and the ITF increases significantly. This result confirms that the non-ENSO variability of ITF comes from the Indian Ocean. However, it is difficult to quantify the Indian and Pacific Ocean SSH's relative importance on ITF's interannual variability. There are two primary reasons; first, very few direct observations of Indonesian throughflow are available. Another reason is that SSHA over the Indo-Pacific oceans that affects the ITF transport on an interannual timescale are positively correlated (Sprintall and Revelard 2014). Hence the in-phase SSH variation in both regions makes it difficult to quantify the influence of respective ocean basins. Sprintall et al. (2014) also pointed out that the Indian ocean dynamics play a major role compared to Pacific Ocean dynamics in drawing collective transport through the outflow passages during co-occurring ENSO-IOD events. Nidheesh et al. (2013) also show that the leading mode of SSH anomalies

on the inter-annual time scale displays comparable loadings indicating the unchanged SSH gradient across the Indonesian Islands. These negatively correlated surface winds and comparable SSHA over the NWP and SEI regions result in an equal contribution to ITF variability from both the oceans on an interannual timescale.

Contrary to the significant correlation on inter-annual timescale, surface wind variation over the two basins is relatively independent. Although Lee and McPhaden (2008) found a negative correlation in the recent inter-decade change between 1993-2000 and 2000-2006 over the surface winds in the two basins, Nidheesh et al. (2013) show that the decadal surface wind variations are relatively independent over the two basins for a more extended period (1959-2009). The varying relationship between the Pacific and the Indian Ocean and different study periods could be the reasons for inconsistent results among previous studies. Nidheesh et al. (2013) also show that the SSHA shows significant loadings over the NWP region while subtle loadings over the SEI region on a decadal timescale. These studies suggest that the NWP region significantly contributes to the decadal ITF variation compared to the SEI region. These studies suggest the large contribution to decadal variation of ITF is from the Pacific Ocean only. Hence, the changes in the ITF transport on decadal timescale can be tracked with changes only in the Pacific Ocean or atmospheric winds over the Pacific Ocean.

Studies so far indicated the large contribution from the Pacific Ocean to the decadal variation of ITF transport. However, no research has yet quantified the contribution. Hence, this chapter aims to estimate the contribution from the Pacific and Indian Oceans to the decadal variation of ITF transport using reanalysis and CMIP5 data. Further the studies consistently show the changes in the fundamental basement of the climate system. These changes can affect the contribution from the NWP and SEI regions to the ITF variation on decadal timescale. Hence, we also examined the future changes in the contribution from these

regions to the decadal ITF transport and explored the large-scale wind dynamics behind these changes.

## 4.2 Results

### 4.2.1 Relative contribution from the Indo-Pacific Sea surface height to the ITF transport on decadal variation

The analysis done in the previous sections confirms the idea that the SSHA difference between the Pacific and Indian Oceans explains the ITF variation to a reasonable extent. However, due to a significant difference in the Pacific and Indian Oceans SSH variance, the Pacific and Indian Oceans' contribution to the decadal variation of the ITF transport is also significantly different. To understand the contribution from NWP and SEI regions to the decadal phases of the ITF variation, the positive phases of the ITF are defined as the anomalous volume transport greater than one standard deviation and the negative phases as the anomalous volume transport lesser than one standard deviation. Based on the SSHA variability of the ORAS4 dataset over 612 months from 1959 to 2009, 128 (87) months are selected for the positive (negative) phases as the observed reference of the current climate.

Composites of the SSH anomaly difference between positive and negative ITF phases in the ORAS4 reanalysis (1959-2009) dataset are presented in Figure 4.1. Anomalously positive SSHA over the NWP region and negative SSHA over the SEI region in the difference map of ITF phases indicates the higher volume transport is associated with the distinct SSHA pattern over NWP and SEI regions. However, the magnitude of the anomalies over the NWP and SEI regions are very different. The difference in the SSH anomalies between the NWP and SEI regions is as large as six times compared to SSHA over the SEI region, reflecting that the NWP region has a significantly large contribution in pushing the water from the Pacific Ocean into the Indian Ocean. Meanwhile, SSHA over the Indian Oceans has a significantly smaller contribution in

drawing the water from the Pacific Ocean.

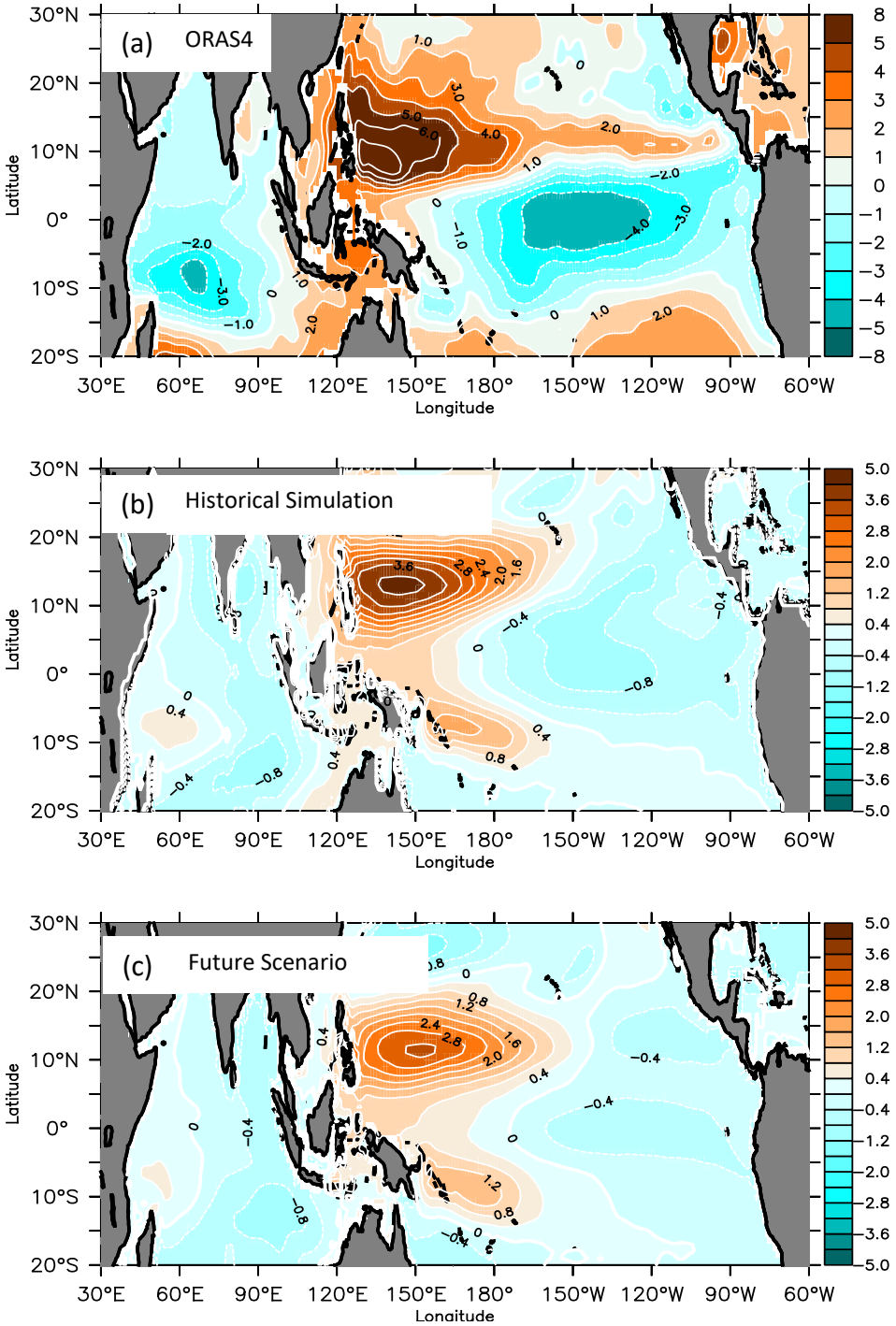


**Fig. 4.1** (a) Composite maps of the difference between positive and negative phases of the decadal SSHA (contoured for every 1.0 cm) based on the ORAS4 dataset. (b) As in (a), but for the multi-model ensemble, decadal SSHA in the historical simulations of the selected CMIP5 models. (c) As in (a), but for the decadal SSHA in the RCP8.5 simulations of those models. The coloring convention is shown on the right of the panels, respectively.

## A. CMIP5 Historical Simulation

Historical simulations in the selected 13 CMIP5 models were analysed to check if they have good skill in representing the high relative contribution from the NWP region and low/negligible contribution from the SEI region to the decadal ITF variation. Similar to the phase selection based on ORAS4 data, the standard deviations of ITF for each CMIP5 model were calculated, and 922 (980) months were selected from 13 of the historical simulations over 7332 months (13 models × 47 years × 12 months) as positive (negative) phases of ITF. Figure 4.1a shows a composite map of SSHAs difference between the positive and negative phases for the ORAS4 dataset. As expected from the definition, a coherent pattern with higher SSHA in the western North Pacific than in the Indian Ocean is found.

**Table 4.1** Spatial correlation coefficients of difference composite SSHA maps among the three datasets, such as the ORAS4 reanalysis dataset (Fig. 4a), the multi-model ensemble mean of the historical simulations (Fig. 4b), and one of the RCP8.5 simulations (Fig. 4c) from the selected CMIP5 models. While values in the middle column indicate the spatial coefficients over the whole domain of the figures (30°S–30°N), the ones in the right column are over a domain only in 20°S–30°N.

| **Datasets** | **30°S-30°N** | **20°S-30°N** |
|---|---|---|
| ORAS4–historical | 0.55 | 0.62 |
| ORAS4–RCP8.5 | 0.41 | 0.50 |
| historical– RCP8.5 | 0.81 | 0.82 |

A similar SSHA pattern is found in the difference composite map based on the historical simulations of the selected CMIP5 models (Fig. 4.1b), even though positive anomalies over the NWP and negative ones over the SEI regions are weaker than those of the ORAS4 dataset (Fig. 4.1a). While the spatial correlation coefficient between Figs. 4.1a and 4.1b is 0.55, and the correlation becomes significant (0.62) when the domain is limited to 20$^{o}$S–30$^{o}$N (upper row in Table 4.1). This significant spatial correlation indicates that the simulated SSHA pattern associated with decadal ITF variations based on the selected CMIP5 model is adequately reproduced. Similar to ORAS4, the large SSHA difference across the Indonesian Islands is mostly attributable to the SSHA over the NWP region. The SEI region's relative contribution is approximately one-sixth of the contribution from the NWP region, which reasonably agrees with the result of the ORAS4. As shown in Fig. 4.1a and 4.1b, the direct and estimated SSHAs over the NWP region in the CMIP5 historical simulation are underestimated than in the ORAS4 (first and second rows of Table 4.2). As indicated in Table 3.1, the climatological mean SSH difference is smaller in ten models among the selected 13 CMIP5 models than in the ORAS4. This implies that the contribution from the NWP tends to be underestimated in most of the selected models. This underestimation in the historical simulations is mainly attributed to the weaker atmospheric wind forcing in the simulated mean states (Lyu et al. 2016).

## B. CMIP5 RCP8.5 Scenario

To understand the future changes in the relative contribution from the NWP and SEI regions to the decadal ITF variation during 2045-2095, the same procedure was followed for selecting the positive and negative phases of the ITF variation on the decadal timescale. 985 (1208) months are selected from 13 of the RCP8.5 simulations over 7332 months as a positive (negative) phase in the future climate. Although, the spatial correlation in the composite difference maps of the SSHA is still high (second row in Table 4.1) between the RCP8.5 (Fig.

4.1c) of the selected CMIP5 models and the ORAS4 as well as between the historical and RCP8.5 simulations (bottom row in Table 4.1). A closer look at the SSHA magnitudes, specifically over the NWP and SEI regions, shows decreased changes in the relative contributions of the direct SSHA over the NWP region from 3.34 cm in the historical simulations to 2.50 cm in the RCP8.5 simulation (a 25% decrease) as well as the increased changes over the SEI region from −0.51 cm to −0.75 cm (a 47% increase). Comparable changes are also found in the estimated SSHA from 2.26 cm to 1.67 cm in the NWP region (a 26% decrease) and from −0.71 cm to −1.00 cm in the SEI region (a 41% increase). Table 4.2 summarizes these changes in the relative contributions in the multi-model ensemble mean and individually selected models. It is important to note that these comparable results in the direct and estimated SSHAs in the individual models and the model ensemble mean strongly indicate that future changes in the relative contributions of the SSHAs across the Indonesian islands are attributable to changes in the atmospheric forcing.

### 4.2.2 Dynamics behind the changes in the contribution from the Pacific and Indian Oceans.

As displayed in Fig. 3.1, identical features in the decadal variability of the direct and estimated SSHAs indicate that the decadal surface wind variability is a major driver to induce the direct SSHAs in Fig. 4.1. In addition, the comparable values of the direct and estimated SSHA in Table 4.2 additionally prove this notion. Hence, to discuss the causes of future changes in the relative contributions of the SSHAs on either side of the Indonesian Islands, the difference composite maps of the multi-model ensemble mean wind stress curl anomalies over the North Pacific (Fig. 4.2) and zonal wind stress anomalies over the Indian Ocean (Fig. 4.3) are plotted.

**Table 4.2** Difference composite values of the direct and estimated SSHAs in the NWP and SEI regions based on the ORAS4 and the multi-model ensemble mean of the selected CMIP5 models with their standard deviation. The bottom row indicates the future changes of the composite values from the historical simulation to the future simulations under the RCP8.5 scenario.

| **Region** | **NWP** | | **SEI** | |
|---|---|---|---|---|
| Data | Direct (cm) | Estimated (cm) | Direct (cm) | Estimated (cm) |
| ORAS4 | 6.23 | 5.72 | 0.30 | -0.70 |
| Historical | 3.34 ± 1.39 | 2.26 ± 1.52 | -0.51 ± 0.71 | -0.71 ± 0.81 |
| RCP8.5 | 2.50 ± 1.21 | 1.67 ± 1.32 | -0.75 ± 0.88 | -1.00 ± 1.12 |
| Future Change | -25% | -26% | 47% | 41% |

In the historical simulations, negative wind stress curl anomalies are significant over the zonal band in 6−16ºN over the North Pacific (Fig. 4.2a), which is associated with anticyclonic surface wind anomalies over the subtropical North Pacific (not shown here). Indeed, the weak anticyclonic surface winds over the subtropical Pacific were illustrated during the positive phase of the PDO (Mantua et al. 1997). These negative wind stress curl anomalies become much weaker in the RCP8.5 simulation than in the historical climate simulation (Fig. 4.2b, 4.2c) due to reduced amplitude of the PDO (Saenko 2005 & Fang et al 2013). This reduced magnitude of wind stress curl anomalies over the NWP region will reduce the magnitudes of wind-forced Rossby waves, which mainly explains the reduced relative contribution of direct and estimated SSHAs over the NWP region during the future climate.

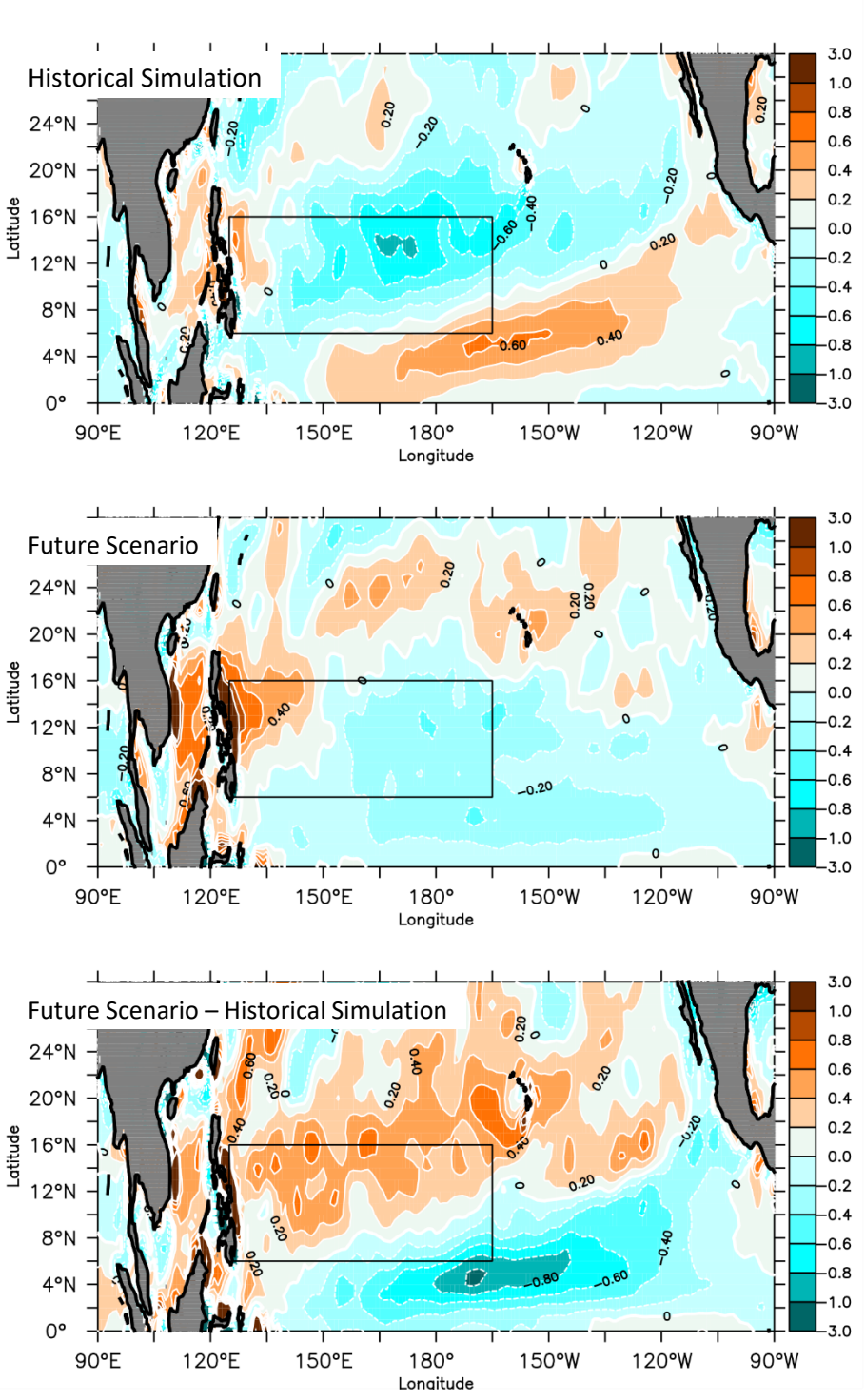


**Fig. 4.2** (a) Difference composite maps of the decadal wind stress curl anomalies (contoured for every 0.2 N $m^{-3}$) based on the multi-model ensemble mean of selected CMIP5 historical simulations. The overlayed box 125°E-165°W, 6-16°N indicates the atmospheric region that affects the SSHA variability in the NWP region. The coloring convention is shown on the right of the panels. (b) As in (a), but for the simulations under the RCP8.5 scenario. (c) is the difference between (b) and (a).

As displayed in Fig. 2.8, negative zonal wind stress anomalies over the central equatorial Indian Ocean significantly contribute to the negative SSHA over the SEI region through the wind-forced equatorial Kelvin wave. The difference composite map of the zonal wind stress anomalies over the Indian Ocean shows enhanced easterly wind stress anomalies over the central equatorial Indian Ocean in the RCP8.5 simulation than in the historical simulation by +23% over the SEI region, which results in stronger negative SSHA. Compared to historical simulations, the analysis also shows the eastward shift of zonal wind stress anomalies (Fig. 4.3) in the future climate scenario. While the zonal wind stress anomalies center is around 70$^{o}$E longitude in the historical climate simulation, it is shifted eastward around 82$^{o}$E in the RCP8.5 simulation. The combined effect of increased amplitude of zonal wind stress anomalies and eastward shift in the anomalies can explain the increased SSHA over the SEI region by +47% in the direct SSHA and +41% in the estimated SSHA (Table 4.3) and, eventually, increased contribution from the SEI region to the decadal variation of ITF transport.

The dynamics behind the enhanced amplitude of the zonal easterly wind stress can be explained with the help of Cai et al (2013) study. In future warming climate the CMIP5 models consistently project sea surface temperature warming. However, in the Indian Ocean, the SST warming pattern will be similar to Positive Indian Ocean Dipole (Cai et al. 2013), resulting in less SST warming in the south-eastern Indian Ocean, compared to western Indian Ocean. This anomalous west-minus-east SST gradient leads to stronger easterlies over the equatorial Indian Ocean and off Java-Sumatra islands, resulting in shallower thermocline off the Java-Sumatra coast to a depth whereby upwelling cools the SST further. The SSTA amplitude off the Java-Sumatra islands enhances due to the higher sensitivity of shallower thermocline to wind anomalies. With the enhancement of the SSTA amplitude in the eastern Indian Ocean, the coupled surface equatorial zonal wind amplitude also enhances.

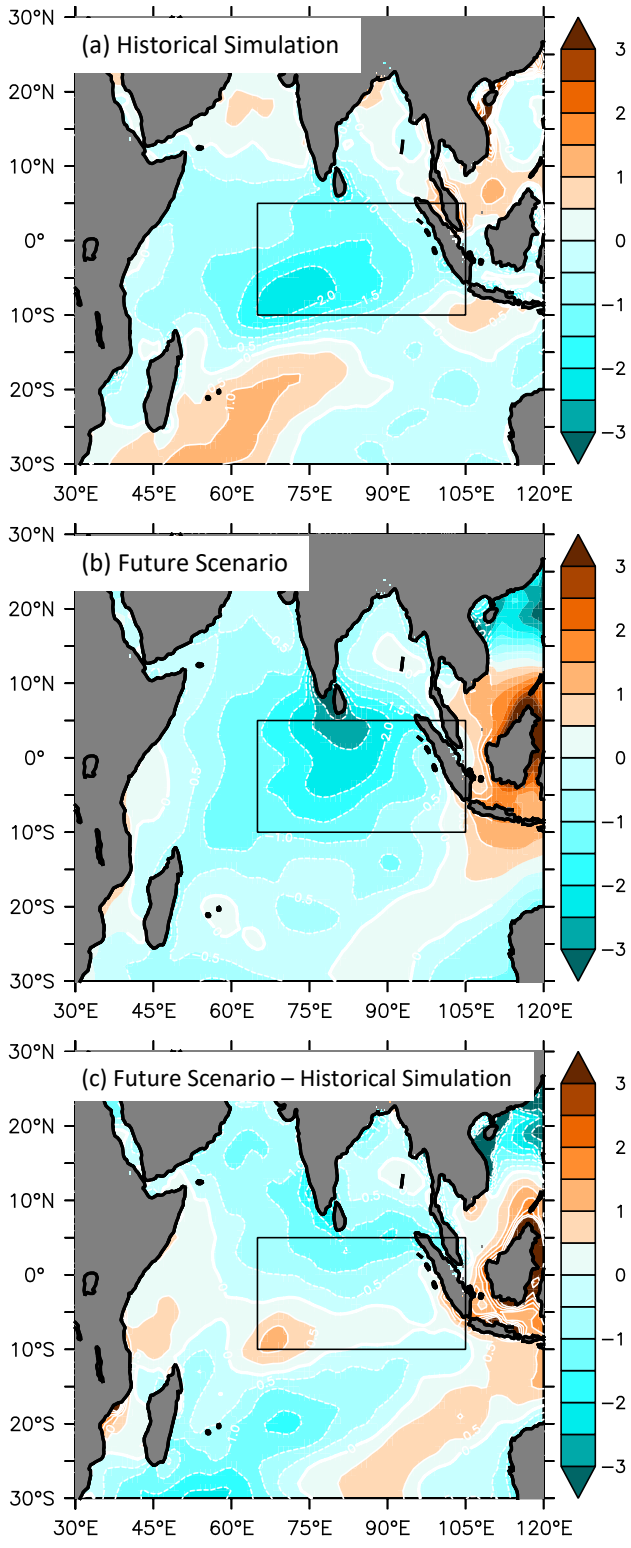


**Fig. 4.3** As in Fig. 4.2, but for zonal wind stress anomalies (contoured for every 0.5 N $m^{-2}$) and the overlayed box 65-105E, 5°N-10°S indicates the atmospheric region that affects the SSHA variability in the SEI region.

## 4.4 Summary and discussion

SSH differences between the NWP and SEI regions drives the ITF. However, the ITF volume transport remains unchanged due to almost comparable amplitude in the SSHA amplitude on an inter-annual timescale. In contrast, many studies show a significant difference in the SSHA over the NWP and SEI regions on a decadal timescale, suggesting a different contribution from the NWP and SEI regions to the ITF variation on a decadal timescale. To understand the relative contribution from these regions, a difference composite map of SSHA between positive and negative phases of the ITF on a decadal timescale was examined.

The ORAS4 reanalysis data and CMIP5 historical simulation show large amplitude over the NWP region and insignificant anomalies over the SEI region. These anomalies are consistent with our understanding of decadal ITF variation. However, with changing climate, the changes in the fundamental basement of the climate may result in changes in the contribution from the NWP and SEI regions to the decadal variation of the ITF. The composite difference map of SSHAs in the future climate scenario (RCP8.5) reveals that the contribution from the NWP and SEI regions is projected to change due to the atmospheric wind forcing changes. These changes include the reduction in the wind stress curl over the NWP region, which decreases the contribution of the NWP region by 25% (26%) as projected in direct (estimated) SSHA. The increased contribution from the Indian Ocean is not only a passive response to the changes in the Pacific Ocean. The zonal wind stress, in the future climate, over the equatorial Indian Ocean show enhanced easterly wind stress, and the region of the higher wind stress is projected to shift eastward. The combined effect of these changes over the Indian Ocean explains the enhanced contribution from the SEI region by 47% (41%) as projected in direct (estimated) SSHA to the decadal variation of the ITF.

# Chapter 5: Conclusion and Discussion

The CMIP5 models project consistent changes in the climate system due to global warming, which may affect the decadal perturbations from the mean state. Hence, we examined the decadal ITF variations and the relative contribution of decadal SSHA variations over the NWP and SEI regions to the ITF in the current and future climate conditions. Decadal timescale analyses of ITF require long-term datasets, which are still unavailable. Hence, a new method is required to estimate ITF's long-term variability. Here, the ITF volume transport was calculated based on monthly mean velocity integrated from the surface to the depth above the bottom on a line from Australia to Indonesia between 9$^{o}$S and 20$^{o}$S along 115$^{o}$E, based on the ORAS4 reanalysis data.

The decadal variability of the ITF is captured by calculating 85-months running mean anomalies that show a significantly high correlation ($r > 0.9$) with the SSHA difference between the NWP and SEI regions. This confirms that the SSHA difference is capable of reproducing the ITF variation on decadal timescales. Further, we reconstruct ITF's decadal variability based solely on wind stress data over the Pacific and Indian Oceans, avoiding the dependence on a complexity of the climate model. Alternatively, the SSHAs were simulated using a simple 1.5 reduced gravity model and 46 years of monthly wind stress data from the Pacific and Indian Oceans. The boundary condition forced by the ITF volume transport in the SEI region was partly built using statistical analysis. The correlation coefficient between reanalysis and estimated ITF based on wind stress in this period is greater than 0.8. However, the SSHAs' relative contribution to the ITF variability on either side of the Indonesia strait is not the same due to the large difference in the SSHA variance. Hence, the contribution of the decadal variability of the Indo-Pacific SSHA on ITF was investigated using ORAS4 reanalysis data from

1959 to 2005.

The contributions from the NWP and SEI regions were estimated based on the difference composite anomalies of SSHAs over the NWP and SEI regions between positive and negative phases of the ITF. The analysis of the historical period (1959–2005) concludes that the SSHA over the NWP region drives ITF variability on a decadal timescale. Meanwhile, the SEI region plays a negligible role. Furthermore, the changes in the contribution from the NWP and SEI regions were studied using thirteen (13) CMIP5 models in historical simulations (1959–2005) and RCP8.5 future scenarios (2049–2095). While the analysis of SSHA suggests that anomalies over the SEI region should increase significantly by +47% (direct SSHA) and +41% (estimated SSHA) in the future climate, the anomalies over the NWP region show a significant decrease by –25% (direct SSHA) and –26% (estimated SSHA). These changes in the anomalies are equivalent to the changes in the contribution from the NWP and SEI regions.

These changes in the contribution from direct/estimated SSHAs over the NWP and SEI regions during future climate scenarios (2049–2095) are driven by changes in the wind stress curl over the Pacific and equatorial zonal wind stress over the Indian Ocean. A decreased amplitude of wind stress curl anomalies over the off-equatorial Pacific, associated with the decreased amplitude of the PDO, decreases the SSHA and, therefore, a contribution reduction in the NWP region. While the increased amplitude of zonal wind stress over the equatorial Indian Ocean contribute to the increased contribution from the SEI region, the eastward shift of the anomalies over the equatorial region also contributes to the increased contribution changes from the SEI region to decadal ITF transport. These changes in the zonal wind stress on decadal timescale are the result of the mean climatic changes in the Indian Ocean. These changes include the supressed warming over the south-eastern Indian Ocean region and the enhanced warming in the western Indian Ocean resulting in the anomalous easterly zonal

wind stress and shallower thermocline in the eastern Indian Ocean. The shallower thermocline becomes more sensitive to the wind changes increasing the amplitude of the SSHA over the interannual and possibly on decadal timescale as well.

These changes in the contribution from the NWP and SEI regions to the decadal variation of ITF have significant importance. Previous studies and this analysis have also shown that in the current/historical climate, ITF can be estimated only with the SSHA over the NWP region without considering the variation in the SEI region. However, with global warming and climate change, the projected contribution changes from the NWP and SEI regions to ITF variability indicate that estimating ITF is difficult without considering future climate variation in the Indian Ocean. While this implication based on the analysis only for the 13 selected models, there is a substantial diversity of the simulated SSHA difference between the NWP and SEI regions among all of the CMIP5 models (Table 3.1). A rationale on this diversity in the simulations including a reversed SSHA gradient should be investigated to further improve the performance in representing the future climatological mean and decadal variability in the climate models.

This study opens possibilities for many new studies. Although, this study was focused on understanding the contribution from the Pacific and Indian Oceans to the decadal variability of the ITF the same study can also be carried out on the inter-annual timescale. Since, both the oceans have almost same contribution to the inter-annual variability of the ITF, it would be interesting to know how this contribution is expected to change in warming climate. With stronger climatological easterly wind stress in equatorial Indian Ocean in future climate, the SSTA amplitude is expected to increase off the Java-Sumatra coast due to the shallower thermocline. This enhanced amplitude of the SSTA further enhances the amplitude of the zonal winds over the equatorial Indian Ocean due to atmospheric coupling.

Understanding the consequences of these changes to the contribution changes from Indian Ocean to inter-annual variation of the ITF would be interesting to study.

In addition, with the refinement of the resolution in the CMIP6 models, it may be possible to use the simulated velocity field in the models and discuss the reproducibility of the ITF in CMIP6 historical simulations and compare the effects of the ITF with observed data. It would also be possible to know if the regions in the Pacific and Indian oceans that affects the ITF variability will change with warming climate.

During the hiatus period the ITF transferred the significant amount of heat from the Pacific Ocean into the Indian Ocean. This increased ITF transport from the Pacific to Indian Ocean have resulted into the influx of increased heat and lower salinity. The western ghats show higher rainfall during the same time period during south-west monsoon season. It would be interesting to know the if the higher rainfall over the western ghats of India during this decade was fuelled by the higher moisture carrying winds from the ITF exit region due to higher temperature and lower salinity.

# References

Abe H, Tanimoto Y, Hasegawa T, Ebuchi N, Hanawa K (2014) Oceanic Rossby waves induced by the meridional shift of the ITCZ in association with ENSO events. J. Oceanogr. 70(2):165-174. doi.org/10.1007/s10872-014-0220-1

Abe H, Tanimoto Y, Hasegawa T, Ebuchi N (2016) Oceanic Rossby waves over eastern tropical Pacific of both hemispheres forced by anomalous surface winds after mature phase of ENSO. J. Phys. Oceanogr. 46(11):3397-3414. doi.org/10.1175/JPO-D-15-0118.1

Anderson DL, Balmaseda M (2005) Overview of ocean models at ECMWF. InProc. Seminar on Recent Developments in Numerical Methods for Atmospheric and Ocean Modelling (pp. 103-111).

Balmaseda MA, Vidard A, Anderson DL (2008) The ECMWF Ocean Analysis System : ORA-S3. Mon. Weather Rev. 136(8):3018-3034. doi.org/10.1175/2008MWR2433.1

Balmaseda MA, Mogensen K, Weaver AT (2013) Evaluation of the ECMWF ocean reanalysis system ORAS4. Quar. J. of the Roy. Met. Soc. 139(674):1132-1161. doi.org/10.1002/qj.2063

Bjerknes J (1969) Atmospheric teleconnections from the equatorial Pacific, Mon. Weather Rev. 97(3): 163-172. doi.org/10.1175/1520-0493(1969)097<0163:ATFTEP>2.3.CO;2

Cai W, Zheng XT, Weller E, Collins M, Cowan T, Lengaigne M, Yu W, Yamagata T (2013) Projected response of the Indian Ocean Dipole to greenhouse warming. Nat. Geosci. 6(12):999-1007. doi.org/10.1038/ngeo2009

Capotondi A, Alexander MA, Deser C (2003) Why are there Rossby wave maxima in the Pacific at 10° S and 13° N? J. Phys. Oceanogr. 33(8):1549-63.

doi.org/10.1175/1520-0485(2003)033<1549:WATRWM>2.0.CO;2

Clark AJ, Liu X (1994) Interannual Sea Level in the Northern and Eastern Indian Ocean. J. Phys. Oceanogr. 24(6):1224-35. doi.org/10.1175/1520-0485(1994)024%3C1224:ISLITN%3E2.0.CO;2

Dee DP, and ERA-Interim team (2011) The ERA-Interim reanalysis: Configuration and performance of the data assimilation system. Quar. J. of the Roy. Met. Soc. 137(656):553-97. doi.org/10.1002/qj.828

Deepa JS, Gnanaseelan C, Mohapatra S, Chowdary JS, Karmakar A, Kakatkar R, Parekh A (2019) The Tropical Indian Ocean decadal sea level response to the Pacific Decadal Oscillation forcing. Clim. Dyn. 52: 5045–5058. doi.org/10.1007/s00382-018-4431-9

Dong L, Zhou T, Dai A., Song. F, Wu B, Chen X (2016) The Footprint of the Inter-decadal Pacific Oscillation in Indian Ocean Sea Surface Temperatures. Sci Rep 6, 21251 doi.org/10.1038/srep21251

Drushka K, Sprintall J, Gille ST, Brodjonegoro I (2010) Vertical structure of Kelvin waves in the Indonesian Throughflow exit passages. J. Phys. Oceanogr. *40*(9), 1965-1987. doi.org/10.1175/2010JPO4380.1

England MH, Huang F (2005) On the interannual variability of the Indonesian Throughflow and its linkage with ENSO. J. of Clim. 18(9):1435-44. doi.org/10.1175/JCLI3322.1

Fu LL, Qiu B (2002) Low frequency variability of the North Pacific Ocean: The roles of boundary-and wind-driven baroclinic Rossby waves. J. of Geophy. Res.:Oceans. 107(C12):13-. doi.org/10.1029/2001JC001131

Gordon AL, Huber BA, Metzger EJ, Susanto RD, Hurlburt HE, Adi TR (2012) South China Sea throughflow impact on the Indonesian throughflow. Geophys. Res. Lett. 39(11). doi.org/10.1029/2012GL052021

Gordon AL, Sprintall J, Van Aken HM, Susanto D, Wijffels S, Molcard R, Ffield A, Pranowo W, Wirasantosa S (2010) The Indonesian throughflow during 2004–2006 as observed by the INSTANT program Dyn. of Atm. and Oce. 50(2):115-28. doi.org/10.1016/j.dynatmoce.2009.12.002

Gordon AL, Susanto RD, Ffield A, Huber BA, Pranowo W, Wirasantosa S (2008) Makassar Strait throughflow, 2004 to 2006. Geophys. Res. Lett. 35(24):3-7. doi.org/10.1029/2008GL036372

Gordon AL, Susanto RD, Ffield A (1999) Throughflow within Makassar Strait. Geophys. Res. Lett. 26(21):3325-3328. doi.org/10.1029/1999GL002340

Han W, Vialard J, McPhaden MJ, Lee T, Masumoto Y, Feng M, De Ruijter, WPM (2014) Indian ocean decadal variability: A review. BAMS 95(11):1679-1703. doi.org/10.1175/BAMS-D-13-00028.1

Kessler WS (1990) Observations of long Rossby waves in the northern tropical Pacific. J. of Geophy. Res.: Oceans. 95(C4):5183-217. doi.org/10.1029/JC095iC04p05183

Kosaka Y, Xie SP, Lau NC, Vecchi GA (2013) Origin of seasonal predictability for summer climate over the Northwestern Pacific. PNAS 110(19):7574-7579. doi.org/10.1073/pnas.1215582110

Li M, Gordon AL, Wei J, Gruenburg LK, Jiang G (2018) Multi-decadal timeseries of the Indonesian throughflow. Dyn. of Atm. and Oce. 84-95.. doi.org/10.1016/j.dynatmoce.2018.02.001

Lee SK, Park W, Baringer MO, Gordon AL, Huber B, Liu Y (2015) Pacific origin of the abrupt increase in Indian Ocean heat content during the warming hiatus. Nat. Geosci. 8(6):445-449. doi.org/10.1038/NGEO2438

Lee T, McPhaden MJ (2008) Decadal phase change in large-scale sea level and winds in the

Indo-Pacific region at the end of the 20th century. Geophys. Res. Lett. 35(1):1-7. doi.org/10.1029/2007GL032419

Lyu, K, Zhang X, Church J.A., Hu J (2016), Evaluation of the interdecadal variability of sea surface temperature and sea level in the Pacific in CMIP3 and CMIP5 models. Int. J. Climatol., 36(11): 3723-3740. doi.org/10.1002/joc.4587

Madec G, and the NEMO team (2008) NEMO ocean engine. Note du Pˆole de mod´elisation, Institut Pierre-Simon Laplace (IPSL), France, No 27, ISSN No 1288-1619. doi.org/10.5281/zenodo.3248739

Mantua NJ, Hare S, Zhang Y, Wallace JM, Francis RC (1997) A Pacific interdecadal climate oscillation with impacts on salmon production Bull. Amer. Met. Soc. 78(6), 1069-1080. doi.org/10.1175/1520-0477(1997)078<1069:APICOW>2.0.CO;2

Masumoto Y (2002) Effects of interannual variability in the eastern Indian Ocean on the Indonesian Throughflow. J. of Oceanogr. 58(1):175-82. doi.org/10.1023/A:1015889004089

Metzger EJ, Hurlburt HE, Xu X, Shriver JF, Gordon AL, Sprintall J, Susanto RD, Van Aken HM (2010) Simulated and observed circulation in the Indonesian Seas: 1/12 global HYCOM and the INSTANT observations. Dyn. of Atm. and Oce. 50(2):275-300. doi.org/10.1016/j.dynatmoce.2010.04.002

Meyers G (1979) On the annual Rossby wave in the tropical North Pacific Ocean. J. Phys. Oceanogr. 9(4):663-74. doi.org/10.1175/1520-0485(1979)009<0663:OTARWI>2.0.CO;2

Meyers G (1996) Variation of Indonesian throughflow and the El Niño-Southern Oscillation. J. Geophys. Res. Oceans. 101(C5):12255-12263. doi.org/10.1016/S0065-3527(08)60734-4

Mogensen K, Balmaseda MA, Weaver A (2012) The NEMOVAR ocean data assimilation system as implemented in the ECMWF ocean analysis for System 4. ECMWF. Tech

Memo. 668:6222-6.

Moss RH, Edmonds JA, Hibbard KA, Manning MR, Rose SK, Van Vuuren DP, Carter TR, Emori S, Kainuma M, Kram T, Meehl GA (2010) The next generation of scenarios for climate change research and assessment. Nature 463:747-756. doi.org/10.1038/nature08823

Murtugudde R, Busalacchi J, Beauchamp J (1998) Seasonal to interannual effects of the Indonesian throughflow on the tropical Indo-Pacific Basin. J. Geophys. Res. Oceans. 103(C10):21425-41. doi.org/10.1029/98JC02063

Nidheesh AG, Lengaigne M, Vialard J, Unnikrishnan AS, Dayan H (2013) Decadal and long-term sea level variability in the tropical Indo-Pacific Ocean. Clim. Dyn. 41(2):381-402. doi.org/10.1007/s00382-012-1463-4

Potemra JT, Lukas R, Mitchum GT (1997) Large‐scale estimation of transport from the Pacific to the Indian Ocean. J. Geophys. Res. Oceans. *102*(C13), 27795-27812. doi.org/10.1029/97JC01719

Potemra JT, Schneider N (2007) Interannual variations of the Indonesian throughflow. J. Geophys. Res. Oceans. 112(5):1-13. doi.org/10.1029/2006JC003808

Power S, Casey T, Folland C, Colman A, Mehta V (1999) Interdecadal modulation of the impact of ENSO on Australia. Clim. Dyn. 15(5) 319–324. doi.org/10.1007/s003820050284

Qiu B, Chen S (2010) Eddy-mean flow interaction in the decadally modulating Kuroshio Extension system. Deep Sea Research Part II: Top. Stud. in Oceanogr. 57(13-14):1098-110. doi.org/10.1016/j.dsr2.2008.11.036

Roxy M, Gualdi S, Drbohlav HK, Navarra A (2011) Seasonality in the relationship between El Niño and Indian Ocean dipole. Clim. Dyn. 37(1), 221-236. doi.org/10.1007/s00382-010-0876-1

Samanta D, Goodkin NF, Karnauskas KB (2021) Volume and heat transport in the South China Sea and maritime continent at present and the end of the 21st century. J. Geophy. Res. Oceans. 126, e2020JC016901. doi.org/10.1029/2020JC016901

Schneider N (1998) The Indonesian Throughflow and the global climate system. J. Clim. 11(4):676-689. doi.org/10.1175/1520-0442(1998)011<0676:TITATG>2.0.CO;2

Schouten MW, De Ruijter WP, Van Leeuwen PJ, Dijkstra HA (2002) An oceanic teleconnection between the equatorial and southern Indian Ocean. Geophys. Res. Lett. 29(16):59-1. doi.org/10.1029/2001GL014542

Song Q, Vecchi GA, Rosati AJ (2007) The role of the Indonesian throughflow in the Indo-Pacific climate variability in the GFDL coupled climate model. J. Clim. 20(11):2434-2451. doi.org/10.1175/JCLI4133.1

Sprintall J, Revelard A (2014) The Indonesian Throughflow response to Indo-Pacific climate variability. J. Geophys. Res. Oceans. 119(1):1365-1382. doi.org/10.1002/2013JC009533

Sprintall J, Wijffels SE, Molcard R, Jaya I (2009) Direct estimates of the indonesian throughflow entering the indian ocean: 2004-2006. J. Geophys. Res. Oceans. 114(7):2004-2006. doi.org/10.1029/2008JC005257

Sprintall J, Wijffels S, Gordon AL, Ffield A, Molcard R, Susanto RD, Soesilo I, Sopaheluwakan J, Surachman Y, van Aken HM (2004) Instant: A new international array to measure the indonesian throughflow. EOS 85(39):369-376. doi.org/10.1029/2004EO390002

Susanto RD, Ffield A, Gordon AL, Adi TR (2012) Variability of Indonesian throughflow within Makassar Strait, 2004-2009. J. Geophys. Res. Oceans 117(9):2004-2009. doi.org/10.1029/2012JC008096

Tillinger D, Gordon AL (2009) Fifty years of the Indonesian Throughflow. J. of Clim. 22(23):6342-55. doi.org/10.1175/2009JCLI2981.1

Tokinaga H, Xie SP, Timmermann A, McGregor S, Ogata T, Kubota H, Okumura YM (2012) Regional patterns of tropical indo-pacific climate change: Evidence of the walker circulation weakening. J. Clim. 25(5):1689-1710. doi.org/10.1175/JCLI-D-11-00263.1

Tozuka T, Qu T, Masumoto Y, Yamagata T (2009) Impacts of the South China Sea Throughflow on seasonal and interannual variations of the Indonesian Throughflow. Dynamics of Atmospheres and Oceans. 47(1-3):73-85. doi.org/10.1016/j.dynatmoce.2008.09.001

Uppala SM, and ERA-40 team (2005) The ERA-40 re-analysis. Quar. J. of the Roy. Met. Soc. 131(612):2961-3012. doi.org/10.1256/qj.04.176

Vivier F, Curie M, Kelly KA (1999) Contributions of wind forcing, waves, and surface heating to sea surface height observations in the Pacific Ocean. J. Geophys. Res. Oceans. 104(C9):20767-20788. doi.org/10.1029/1999JC900096

Vranes K, Gordon AL, Ffield A (2002) The heat transport of the Indonesian throughflow and implications for the Indian Ocean Heat Budget. *Deep-Sea Res*. 49, 1391–1410. doi.org/10.1016/S0967-0645(01)00150-3

Watanabe M, Kamae Y, Yoshimori M, Oka A, Sato M, Ishii M, Mochizuki T, Kimoto M (2013) Strengthening of ocean heat uptake efficiency associated with the recent climate hiatus. Geophys. Res. Lett. 40(12):3175-3179. doi.org/10.1002/grl.50541

Watanabe WB, Ilson CA (2016) Can a minimalist model of wind forced baroclinic Rossby waves produce reasonable results? Ocean Dyn. 66(4):539-548. doi.org/10.1007/s10236-016-0935-1

Wijffels S, Meyers G (2004) An intersection of oceanic waveguides: Variability in the Indonesian Throughflow region. J. of Phys. Oceanogr. 34(5):1232-53. doi.org/10.1175/1520-0485(2004)034%3C1232:AIOOWV%3E2.0.CO;2

Wijffels SE, Meyers G, Godfrey JS (2008) A 20-yr average of the Indonesian Throughflow: Regional currents and the interbasin exchange. J. of Phys. Oceanogr. 38(9):1965-78. doi.org/10.1175/2008JPO3987.1

Wolff JO, Maier-Reimer E, Legutke S (1997) The Hamburg Ocean primitive equation model HOPE. ISSN 0940-9327

Wyrtki K (1987) Indonesian through flow and the associated pressure gradient. J. Geophys. Res. Oceans. 92(C12):12941-12946. doi.org/10.1029/JC092iC12p12941